SOFT-SEDIMENT AND HARD-ROCK DEFORMATION
IN THE CHINLE FORMATION, NORTHEASTERN ARIZONA

A Thesis

by

Jay Roger Scheevel

Submitted to the Graduate College of
Texas A&M University
in partial fulfillment of the requirements for the degree of

MASTER OF SCIENCE

August, 1983

Major Subject: Geology

SOFT-SEDIMENT AND HARD-ROCK DEFORMATION
IN THE CHINLE FORMATION, NORTHEASTERN ARIZONA

A Thesis

by

Jay Roger Scheevel

Approved as to style and content by:
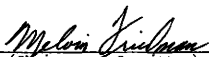
_____
(Chairman of Committee)
    Melvin Friedman

_____   _____
    (Member)   (Member)
    Brann Johnson
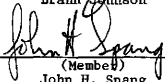
_____   _____
    (Member)   (Department Head)
    John H. Spang   Robert J. Stanton

August, 1983

1812066

ABSTRACT

Soft-sediment and Hard-rock Deformation of the Chinle Formation,

Northeastern Arizona

(August 1983)

Jay Roger Scheevel, B.S., University of Illinois;

Chairman of Advisory Committee: Dr. Melvin Friedman

The Triassic Chinle Formation of Northeastern Arizona is studied with a view toward distinguishing between features formed as a result of soft-sediment (Triassic) and hard-rock (Laramide) deformation. In outcrop both types of deformation have similar structural style and scale. Soft-sediment and hard-rock localities were chosen initially by their proximity to large monoclines, i.e., to obvious tectonic features. The only macroscopic features unique to soft-sediment deformation are soft-sediment small-faults with up to 2 cm of dip-slip displacement at high angles to bedding. These fault arrays form in orthorhombic symmetry with respect to strike and dip of bedding. The macroscopic features unique to hard-rock deformation are: (1) open fractures oriented normal to bedding, with little or no offset, and locally high abundances (30/meter) as composite arrays which are more ordered with respect to regional coordinates than to

bedding strikes; and (2) hard-rock small-faults (fault-zones 1-3 mm wide) which show up to 2 cm of offset at any angle to bedding, appearing as reverse-weathering bands of comminuted sand grains. Features which are ambiguous as to deformation-type are: (1) chevron-folds (1 to 300 m wavelengths), (2) decollement or truncated surfaces, (3) plunging folds, (4) slickensided shear-surfaces in claystones.

Microscopic observation of the deformed sandstones reveals that the order and abundance of the following are diagnostic of hard-rock deformation: (1) sharp extinction boundaries in quartz, (2) microfractures, (3) deformation lamellae in quartz, (4) undulatory extinction in quartz, (5) calcite twin-lamellae. Correlations between clay models and their natural counterparts indicate that soft-sediment small-faults form due to bending stresses. Rock models deformed at elevated confining pressures suggest that the Chinle acted as a detachment horizon in the Laramide, producing intraformational deformation of the same style as earlier soft-sediment deformation.

ACKNOWLEDGEMENTS

DEDICATION

I dedicate this work to my parents Robert and Janet Scheevel who taught me to be inquisitive.

TABLE OF CONTENTS

TABLE OF CONTENTS (continued)

TABLE OF CONTENTS (continued)

LIST OF TABLES

LIST OF FIGURES

LIST OF FIGURES (continued)

LIST OF FIGURES (continued)

LIST OF FIGURES (continued)

CHAPTER I

INTRODUCTION

Significance of the Study.

This study characterizes the structural behavior of a bentonite-
rich formation which deformed as a soft-sediment by gravity processes
soon after its deposition in the Triassic, and later after burial
and lithification, as a hard-rock during the Laramide. The primary
importance of the study is that it points out the striking macro-
scopic similarities of the structures produced under both deforma-
tional regimes, as well as important field and laboratory criteria
for distinguishing their origin.

Objectives.

The objectives of this study are to (1) analyze the geometry,
kinematics and dynamics of deformation of the sandstones and

The style and format of this thesis follow that of the Bulletin
of the Geological Society of America.

claystones[1] of the Chinle Formation of Northeastern Arizona, on a variety of scales, in both the field and the laboratory; (2) demonstrate applicable criteria for distinguishing between "soft-sediment" (Triassic) and "hard-rock" (Late-Cretaceous) deformation of these rocks; (3) estimate the relative mechanical behaviors of the lithologies studied, under the inferred deformational conditions; and (4) evaluate the validity of loading conditions interpreted from (1). Integral to (4) will be the use of experimental, physical models involving a variety of loading conditions and material components.

Structures Studied.

The principal structures studied are symmetrical and assymmetrical folds with shallow or steeply dipping limbs. The folds range from 1 to 300 m or more in wave length. Often they do not have well-exposed or preserved hinges. The folds may be truncated by horizontal surfaces of similar lithologies. The folded units are often cut by reverse faults which do not transgress the formation boundary. Most of these folds and faults are found only in the lower-most member of the Chinle formation. Because the claystone in the folded units is usually poorly exposed, the majority of the study was carried out through observation of the sandstones.

---

(1) In this study the term claystone is used in lieu of terms such as "highly bentonitic siltstones and shales"; this is done to emphasize the smectite clay content (up to 90%) of the rocks, a characteristic which has critical importance in the structural behavior of the formation.

Some of the structures are unquestionably due to soft-sediment processes (probably gentle-slope and gravity-induced), as indicated by their location distant from large tectonically-induced structures of Laramide age (e.g. Figure 1, near St. Johns). Other features of similar macroscopic character in the Chinle, are undoubtably the result of Laramide deformation as evidenced by their proximity and geometric relationship to Laramide structural features (e.g. Figure 1, near Ft. Defiance).

Distinction between the various causes of similar structures in both settings is a key goal of the study. In support of this, use of recent studies of microscopic deformation mechanisms and the relationships of micro-and macroscopic deformation mechanisms in rocks are valuable for meaningful interpretation of deformation features at all scales. Mechanical conditions interpreted from the microstructures constitute the groundwork for reinforcing field observations regarding the genesis of the macroscopic deformation features.

Geological Framework.

The Late Triassic Chinle Formation of Northeastern Arizona is composed of sequences of redbeds (Figure 2). The formation has a large areal extent being found in parts of Arizona, Nevada, Utah, Colorado, and New Mexico but is generally limited to within the boundaries of the Colorado Plateau physiographic province. The formation varies from a feather-edge thickness on several boundaries to a maximum thickness of approximately 500 m near Ft. Wingate, New

Figure 1. Location Map of study area shows locations of major Laramide structural features (monocline symbols). Stippled areas are areas observed for this study.
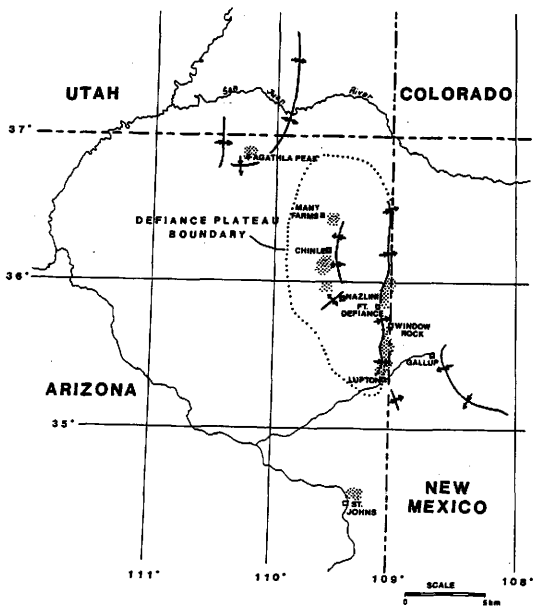
Figure 2. Stratigraphic column of Chinle and encompassing form-
ations near Ft. Defiance, Arizona.

THICKNESS
(APPROX.)

WINGATE FM.-ROCK POINT MBR. (TRIASSIC)
MASSIVE TO LAMINATED SILTSTONE

50M

55M

OWL ROCK MBR.
INTERCALATED SILTSTONE AND
FRESH-WATER LIMESTONE

BOUNDARY INDISTINCT

UPPER PETRIFIED FOREST MBR.
RED AND VARIGATED CLAYSTONE

CALCAREOUS
BENTONITIC

CORREAL SANDSTONE (?)
RED QUARTZOSE SANDSTONE

185 TO
310M

OCCASIONAL LIME-PEBBLE CONGLOMERATE

CHINLE FM. (TRIASSIC)

SONSELLA SANDSTONE
FLUVIAL QUARTZOSE SANDSTONE

80225M

50M

LOWER PETRIFIED FOREST MBR.
VARIGATED CLAYSTONE TO SILTSTONE

MONITOR BUTTE MBR.

60M

FINE-GRAINED SANDSTONE AND CLAYSTONE

20M

SHINARUMP MBR.
SANDSTONE AND CONGLOMERATE

DE CHELLEY FM. (PERMIAN)
CROSS-BEDDED DUNE SANDSTONE

160M

Mexico. The Chinle is composed of many members which vary in nomen-
clature geographically. Stewart and others (1972) have divided the
formation into two basic components for purposes of provenance
analysis. This division provides a useful structural division in
that it separates the silty, calcareous, upper red-bed portion of
the Chinle Formation from the lower, largely bentonitic portion.
Part of the lower bentonitic sandstone and claystone portion, the
Monitor Butte member, commonly contains the most abundant examples
of the type of structures under investigation. Stewart and others
(1972) show the thickness of the lower bentonitic part of the Chinle
to be between 220 and 370 m in the vicinity of the Defiance Plateau
(Figure 1, p. 5). This bentonitic section is unique in composition
relative to the rocks immediately above and below it (mostly
"blanket" sandstones and siltstones). The deformational features
found in the Chinle also are unique to the section in the region,
perhaps due to the well known contrasts in strength and ductility
between sandstones and claystones.

The Chinle Formation was deposited in a flood plain, swamp and
shallow lake environment (Stewart and others, 1972; Reppening and
others, 1969; Cooley, 1957). The lithologies in the bentonitic por-
tion of the Chinle are fluvial and lacustrine-deltaic sandstones, and
claystones. Many of the individual sand bodies in the lower Chinle
are not traceable over large distances due to facies changes, poor
outcrop and deformation. However, the gross uniformity of composi-
tion, lithologic sequences and localized but regionally distributed
intraformational structural features further suggest that the

mechanical behavior of the Chinle Formation was uniform throughout its areal extent. For example, identical lithologies are similarly folded rotated and truncated in the same stratigraphic position (Monitor Butte Member), on the same scale across an area between Capitol Reef State Park, Utah and St. Johns, Arizona, a distance of more than 320 km (R. E. Thaden, personal communication, 1980).

Deformation of the Chinle Formation has not been extensively studied in Northeastern Arizona. The folding and truncation of the lower-most member of the formation has been documented by studies of Reppening and others (1969), Cooley (1957), and Stewart and others (1972). They all conclude that the deformation occurred contemporaneously with deposition when the Chinle was largely unconsolidated, i.e., soft-sediment deformation. Reppening and others found, on the basis of thickness variations, that the deformation may have been related to local uplift. That is, the deformation and thinning possibly were due to local uplift at or near the time of deposition (Late Triassic). The only specific study of this deformation was made by Green (1956), who mapped and described folds in an area of outcrop of lower Chinle, northeast of St. Johns, Arizona. He concentrated primarily upon description of fold morphology and possible scenarios for their development, and concluded that the folds were the result of slumping of an over-steepened lake delta. Although Green observed only one locality, his study describes folds and lithologies quite similar to those found in the field area of the present study.

Deformation of the Chinle Formation during the Laramide, i.e.

subsequent to the soft-sediment phase, has not been studied in great detail, with descriptions of the nature of deformation restricted only to regional accounts, none of which consider the Chinle individually.

Definitions.

In order to describe the deformation of the Chinle effectively it is necessary to define criteria which permit recognition of the different origins of geometrically similar deformational features. Accordingly, a major element of this study is the definition of the terms "soft-sediment" and "hard-rock" deformation. An understanding is necessary of how the mechanical properties of rock-materials which fall into the two classifications vary and what is the consequent effect on the observed deformational features on all scales.

Soft-sediment Deformation.

This is defined as the deformation of uncemented sediments during or soon after deposition and usually at or near the surface. Processes include gravity slumping, high pore-pressure diapirism, differential compaction, liquifaction, and desiccation. In the study area, soft-sediment deformation of the Chinle in Late Triassic is attributable to gravity-induced slumping and gliding, probably the result of unstable lake deltas (Green, 1956).

Hard-rock deformation.

This term will be used to cover all deformational events that are not in the soft-sediment category, and which in the study area produced the folds and faults of the Laramide orogeny (Late Cretaceous-Early Tertiary). Unlike soft-sediment deformation the hard-rock classification actually makes no restrictions on the age of the rocks which are deformed, or the physical locale or environment of the deformation.

Associated Rock-properties.

With the definitions of hard-rock and soft-sediment deformation go implicit generalizations about the nature of the rock and its deformational environment. Hard-rock deformation of the Chinle in the Laramide is estimated to have taken place at a depth of approximately 2,000 m or greater. Burial of rock imposes an effective confining pressure on the rock which is ideally equal to the weight of the overlying rock column minus the pore-fluid pressure in permeable rocks (Handin and others, 1963). Due to the great amount of low permeability claystone, it is possible that there may have been high pore-pressures trapped in the sometimes lenticular sandstones of the Chinle during hard-rock deformation. If this was the case, then the effective confining pressure would have been somewhat less than estimated below. Compaction accompanying burial produces a decrease in porosity and permeability of an aggregate, as well as an increased frictional and solution-induced interlocking of grains. All of these effects tend to increase rock strength (e.g., Dunn and

others 1973). Also accompanying burial is an increase in temperature dependent in magnitude on the thermal gradient at that locality. The effect of temperature is to increase ductility and decrease strength (Heard, 1963). The estimated effective confining pressure, in Late Cretaceous time is about 22 MPa, assuming that pore fluids (water) communicated with the surface and a depth of burial of the Chinle of 2000 m. The estimated temperature with a normal geothermal gradient (27.5-37.5°C/Km) is 80-100°C. Temperatures higher than 100°C are also inconsistent with preservation of the observed smectite content. Based on the work of Handin and others (1963), 22 MPa is considered sufficient pressure to strengthen the rocks of the Chinle noticably, however 100°C is considered insignificant temperature to appreciably weaken the same rocks.

The chemistry of the pore fluid can also affect the mechanical properties of the rock (e.g., Swolfs, 1971). The magnitude of the effect is expected to be small and estimation of its effect is beyond the objectives of this study.

Soft-rock environments of deformation in the Chinle necessarily exclude almost all of the above property modifications due to burial and might be expected to induce only slightly tighter packing and a slightly greater cohesion between grains prior to deformation. Evidence presented in this study suggests that no cementation occurred prior to soft-sediment deformation.

Deformational Criteria.

Soft-sediment deformation.

Macroscopic features related to soft-sediment deformation that
have been observed in rocks like those of the Chinle are as follows:

(1) Kliest (1974) studied features in sandstones and shales of
the Coastal-Belt Franciscan Group in California and concludes
they were formed by depositional slope processes. He found a
unit traceable along strike for 35 km which showed deformational
features typical of argille scalliose: the claystones showed
intensely developed slickensided shear-surfaces. The sandstones
exhibited pull-apart structures with rounded terminations. He
also found cases of sharp truncations between deformed and un-
deformed beds, and undeformed burrow-tubes transecting small
folds in sandstone.

(2) Thomsen (1969) investigated the Tesnus Formation sandstones
and shales in West Texas and observed small normal faults with
less than 2 cm of displacement striking parallel to the paleo-
slope.

(3) Sonstegaard (1979) observed similar faults along with small
recumbent folds in silts and sands of glacial origin in western
Norway, and attributes their genesis to stresses generated by
advancing ice.

(4) Straccia (1981) described folds, truncated thin-sands,
sheared glide-planes, and small normaland reverse-faults with
approximately 2 cm of displacement in cores from the deep Wilcox

sands and shales of South Texas. These features he attributes
to soft-sediment faulting and gravity-creep sliding on a large
scale.

(5) Friedman and White (1980) described small normal faults in
cores from Leg 59 of the Deep Sea Drilling Project in the West
Pacific Parece Vela Basin Sediments. Adjacent to some faults
they found fractured feldspar grains indicating some lithifica-
tion and a high stress differences at the time of faulting. In
other cases they also found untwinned and unbroken calcite fos-
sils and unbroken grains that suggest lesser degrees of lithi-
fication and lower stress differences. They conclude that the
faulting was a result of regional tectonic extension of at
least partially-lithified sediments.

Hard-rock deformation.

Descriptions of deformational features commonly attributed to
hard-rock deformational conditions are abundant in the literature.
Authors often relate these features genetically to larger tecton-
ically induced structures of which they are a part. These include
fractures, cleavage, pressure solution features, subsidiary folding,
faulting and small to large scale cataclasis, as well as many intra-
granular deformational features. Many of these have been observed
in rocks similar to those in the Chinle.

For this study, macrofracture abundance and orientation are
used extensively in the field as indicators of hard-rock deforma-
tion. In the laboratory, microscopic hard-rock deformation features

in sandstones are used extensively and more quantitatively.
Accordingly, a summary of past use of microscopic petrofabrics for
analysis of mechanical aspects of rock deformation is given below.

(1) Friedman and others (1980) used the orientation of micro-
fractures produced in uncemented quartz grains to delineate
stress orientations in experimentally induced drape-folds
formed at high confining pressures. Through comparison with
those formed in calcite-cemented sandstones deformed under
similarly high confining pressures, they emphasize that ordered
fracturing increases with the degree induration of the deformed
aggregates.

(2) Carter and Friedman (1965) demonstrate that intracrystal-
line deformation in quartz (deformation lamellae) in naturally-
deformed calcite-cemented sandstones suggests the same orienta-
tion of principal stresses as twin lamellae in the adjacent
calcite cement. Both features relate to stresses expected dur-
ing folding. Thus, an indurated plate of cemented sandstone
was folded rather than an unconsolidated sand.

(3) Friedman and Stearns (1971), show that natural formation
of calcite twin lamellae in naturally deformed limestones and
limey-dolomite of Teton Anticline, Montana, delineate the
principal stress directions which produced at least part of the
macroscopic fracture pattern observed in outcrop.

Ordered development of microscopic features such as those
above indicate that they were formed as a consequence of hard-
rock deformation. This ordered development of microstructures

is of primary importance in this study as it serves to inde-
pendently confirm which of the field-observed macroscopic
features are related to hard-rock deformation.

Size.

Size of a feature is widely used as a primary criterion for the
differentiation between hard-rock and soft-sediment deformations.
Most hardrock features (folds, faults, macrofractures) tend to be
large in scale (greater than 100 m) and often are linked geometri-
cally to regional tectonism. Soft-sediment features, on the other
hand are often smaller and more localized. Soft-sediment features
are usually considered to be completely confined to the outcrop
scale (e.g., 1 to 100 m). However, where the internal deformation
of a tectonic structure is complex, deformation can adopt the same
scale as soft-sediment structures that have developed in the same
rocks earlier. In this case, distinction is complicated by over-
printing of hard-rock and soft-sediment structures. In such cases
size or scale alone are not a useful differentiation criterion.

Studies by Coleman and others (1974), Berg (1979), and Straccia
(1981) show that soft-sediment deformation in sediments similar to
those in the Chinle Formation can occur over large areas (5 km^2).
Similarly, studies by Prucha and others (1965), Wienberg (1977),
Vaughn (1976), and Cook (1975) demonstrate that irregular smaller
scale hard-rock, subsidiary structures can form in response to
larger Laramide folds, in lithologies similar to those of the Chinle
(see especially Prucha and others, 1965; Fig. 30 A, B, C,

p. 989). Due to the possibility of confusing similar deformation features on the basis of scale and form alone, other macroscopic and microscopic criteria are used in this study as additional necessary diagnostic criteria of soft-sediment and hard-rock deformation.

Approach.

Field study.

The first step of study was the field observation of structures in a variety of locations in Northeastern Arizona. All structures were described on the macroscopic scale. A preliminary classification of macroscopic features due to each type of deformation was established on a basis of their proximity and apparent involvement with larger known Laramide structures. These criteria are later confirmed by thin section study of microstructures from the same locations.

Supplemental to the field study is a compilation and geometric analysis of macrofracture abundances and orientations measured in the field. This analysis is included in the discussion of field observations.

Microscopic study.

Oriented thin sections were prepared from samples collected in the field. These sections were observed and microscopic deformation features recorded. Because microscopic petrofabrics have been shown to be very definitive of the type of conditions which produced them,

they can be used to clarify the degree to which each type of deform-

ation influenced the macroscopic features observed in the field.

Model study.

Complementary to the field and microscopic studies, a series of

physical models were constructed and deformed. These models which

vary in scale, geometry, material-properties and experimental condi-

tions, all attempt to help clarify the possible loading schemes and

relative material responses which may have produced the soft-sediment

and hard-rock deformation features found on a variety of scales in

the field.

CHAPTER II

FIELD OBSERVATIONS

Introduction.

Several localities of exposed Chinle Formation in Northeastern
Arizona were selected for detailed study with the goal of describing
and distinguishing between soft-sediment and hard-rock structures.
The strategy was to formulate a set of general field-criteria for
the interpretation of each type of deformation by recognizing fea-
tures common to many localities exhibiting each style of deforma-
tion. By using many localities a more complete data base of common
macroscopic features was assembled. This base would be nearly im-
possible to assemble at any one location due to incomplete exposure.
After observation of a number of such localities qualitative clas-
sification of additional localities was made while in the field.

The method used initially to distinguish between the two types
of deformation is to first observe a heavily deformed locality that
is so distant from major tectonic (Laramide) structural features
(70 km) so as to be certainly unaffected by any hard-rock deforma-
tion. The best such locality is in an area northeast of St. Johns,
Arizona, located 70 km south of the East Defiance Monocline (Figure
1, p. 5). After study of features in this locality, other areas
which are closer to, but still uninvolved in Laramide structures

were observed. After observing these structural features common to
soft-sediment localities, separation of soft-sediment features from
any remaining deformation features involved in Laramide structures
then yields a qualitative assessment of the degree to which each
type of deformation acted on those rocks.

Soft-Sediment Deformation.

     Six localities displaying soft-sediment deformation were stud-
ied. As reasoned above, four of these were chosen so as to be dis-
tant from or uninvolved in major Laramide structures such as the
East Defiance Monocline (Figure 1, p. 5). These four soft-sediment
localities are discussed below. The remaining two which display
overprinting of hard-rock deformational features will be discussed
in later sections.

St. Johns, Arizona.

General description. An area of approximately 5 km^2, located 3 km
east of St. Johns, Arizona (Figure 3), is the best exposed of all
localities studied. Green (1959), who mapped and described this
same area of folds concluded that the deformation was the result of
down-slope slumping and folding of an over-steepened lake delta.
Green did not distinguish structurally significant units on his
maps. In order to delineate specific structural members produced by
slumping and gliding, the area was remapped for this study using
three structural divisions (Figure 4).

Figure 3. Location of the soft-sediment deformation locality
(detailed map area) near St. Johns, Arizona. The double lines
schematically show axial trends of folds in the area.

109°22'5"

US Highway
666

Qt

Qt

Q

Qt

Qt

TRc

Qt

TRc

Q

Qt

TRc

detailed-map
area

Qt

N

Q

US Highway
180

ST. JOHNS
ARIZONA

34°36'

TRc

Scale

0   1   2 km

Q	Young Quaternary deposits
Qt	Quaternary terrace deposits
TRc	Lower Chinle Formation
/	Dominant fold trends
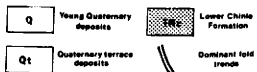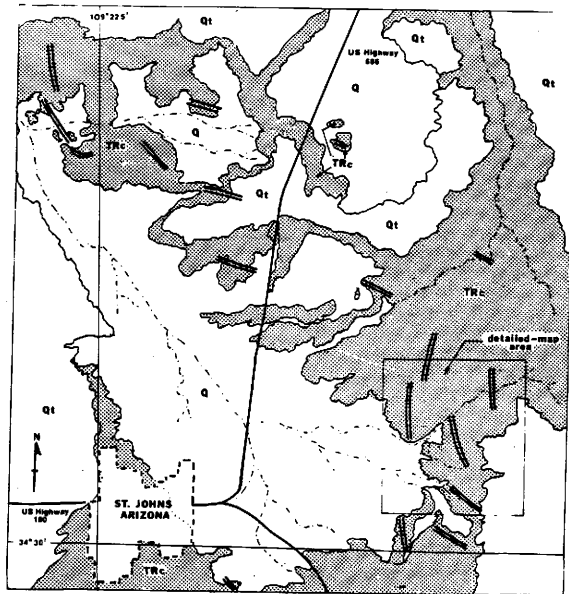
The rocks at this locality consist primarily of calcareous, micaceous, bentonitic, ripple-laminated claystones, siltstones and fine-grained sandstones. These rocks are components of the lower-most member of the Chinle Formation. The sandstones are intercalated with poorly cemented clay and mica-rich beds with less obvious ripple laminations. The intercalation of the two lithologies, as well as more complete quartz-cementation in the clay poor beds, leads to a stair-step weathering pattern. The more resistant quartz-cemented beds weather to greenish brown. Medium-grained, cross-bedded lithic arenites and lime-pebble conglomerates are also present locally but are not as abundant or as traceable as the ripple-laminated sand-stones.

Folds and decollement. Deformed beds are present within a well de-fined zone which varies from approximately 20 m thick in the western-most exposure (Figure 4) to less than 10 m thick to the East. The rocks within the zone are clearly truncated above and below by near-planar, subparallel, slightly westward-dipping (2-3°) shear surfaces (decollements). The rocks within this middle struc-tural unit are folded along a NNW trend (Figure 4). The folds show a general increase in limb dip (from 3-10° to 5-80°) and decrease in wavelength (from 1.0 to .33 km) from east to west. The rocks in the middle structural unit are cut in two places by west-dipping thrust faults (inferred from truncations of resistant weathering sandstone ridges) and in at least one place, by a high-angle (75° east-dip) reverse fault. Folding is almost exclusively chevron in style;

Figure 4. Detailed map of soft-sediment deformation near St. Johns, Arizona.

Qal – Quaternary alluvium
Q – Quaternary alluvial, eolean, or slope deposits
Qs – Quaternary slope deposits
Qls – Quaternary landslide debris
Qt – Quaternary terrace deposit

.... resistant weathering strata
—— drainage

0   .25   .5   1.0 Ka

TRcu – Lower Chinle Fm. upper structural unit
TRcm – Lower Chinle Fm. middle structural unit
TRcl – Lower Chinle Fm. lower structural unit

—— anticlinal axis
—— synclinal axis
—— inferred thrust fault

accordingly very few curved limbs are observed in the deformed beds. The hinge area of the folds are very restricted, and in most instances are either not exposed or are truncated by the planar decollements above and below the zone. The folds are quite often defined in the field only by adjacent limbs which dip in opposite directions. Dips of the axial planes, where they can be defined, are not systematic. However, in the western margin of the Chinle outcrop some of the west-dipping limbs are near vertical or slightly overturned. In map view the folds typically plunge-out along strike.

The sandstones in the middle structural unit display a systematic variation in the intensity of deformation with respect to the thickness of the sandstone unit involved. That is, beds that are the most isotropic, thick-bedded and clay-poor tend to show the least deformation (most widely-spaced fracturing). Beds that are thinnest, most anisotropic and clay rich tend to show the most deformation.

Soft-sediment small-faults[2]. Folding and faulting of the sandstones in the middle-structural unit are typically accompanied by formation of soft-sediment small-faults. Soft-sediment small-faults are essentially planar shear-surfaces oriented at various angles to bedding which have 0.1 to 5 cm of dip-slip displacement. Each fault-plane consists of a zone of disturbed sand grains 0.25 to 1 mm

(2) Assumed to be soft-sediment in origin due to association with structures near St. Johns.

in width across which displacement of current-ripple foresets can usually be traced. There is no evidence for grain breakage or crushing within the fault zones. The soft-sediment small-faults are made obvious in outcrop do to preferential weathering, probably due to a more disordered packing and higher content of calcite and clay along the faults. In the coarse-grained calcite-rich units, the fault zones effervesce with the application of dilute HCl.

Most commonly the soft-sediment small-faults are inclined at 60-80° to bedding and generally strike within 30° of the strike of the bed which contains them. Usually they form sets of conjugate shears which are acutely bisected by the normal to bedding. The detailed geometry of fault sets in any one outcrop is usually quite consistant. Many outcrops show assemblages detailed below.

With rare exception, soft-sediment small-faults observed in this and other soft-sediment localities fall into 3 categories (Figure 5). Since the morphological character of the individual faults-planes themselves is identical (as above), the categorical separation of the different fault arrays is based solely upon their orientations relative to bedding. The first category consists of two conjugate shear planes with strikes parallel to each other and to that of bedding, which intersect at about 60° (Figures 5a, 6). All planes show macroscopically observable offset, identified by displacement of bedding planes. The trace of the line of intersection of an individual fault with bedding is undulatory but grossly consistent. Striations occur on some exposed fault planes that confirm movement down the dip of the fault surface. The effect of

Figure 5. Lower hemisphere, equal-area stereographic projec-
tions of geometries of soft-sediment small fault arrays are: a)
Category 1, poles to fault planes; b) Category 2, poles to fault
planes; c) Category 3, poles to fault planes. Planes marked with
circles have normal displacement and planes marked with X's can have
either normal or reverse displacement relative to bedding. Bedding
strike is marked with a line.
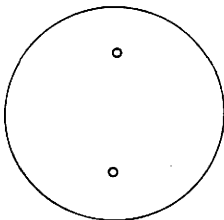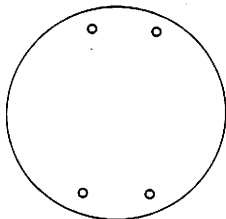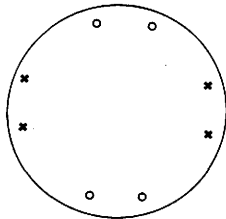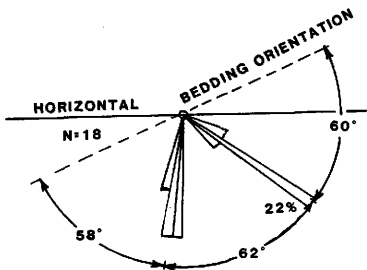
Figure 6. Schematic rose diagram/cross-sectional plot of soft-sediment small-fault orientations at St. Johns (category 1).

the observed displacements is to produce elongation parallel to the bedding dip direction, shortening normal to bedding, and no strain parallel to bedding-strike. This geometry is consistent with a Coulomb-Mohr shear failure where the principal compressive stress is normal to bedding and the least principal stress is parallel to the dip direction.

The second category of fault geometry consists of a four-fault array (Figure 5b, p. 29). Two identical sets of conjugate shear-planes are oriented such that all four faults are in orthorhombic symmetry around three axes: (1) the pole to the bedding; (2) the strike of the bedding; and (3) and dip of the bedding. The acute angle (10 to 30°) between the strikes of the conjugate shear-sets (defined by the angle between their traces on bedding) is bisected by the strike of the host bed. As in category 1 the acute angle between the individual faults of a conjugate-set is bisected by the normal to bedding. The effect of the category 2 fault array is to shorten the bed normal to bedding and extend it principally in the direction of dip and secondarily parallel to strike. This category sometimes is manifest in outcrop by only 3 fault orientations (one of the conjugates is missing in one of the sets). The category 2 fault-array is very similar to that produced experimentally in clays by Oertel (1965), and that proposed theoretically by Reches (1978) to explain faulting in a three dimensional strain field.

A third category of faults is defined by the addition of more sets of conjugates, also in orthorhombic symmetry relative to bedding directions, which show either normal or reverse senses of

displacement (Figure 5c., p. 29). No faults of this category (category 3) were observed at the St. Johns locality, and details of their geometry will be covered in the description of the Many Farms locality.

Faults not falling into one of these three catagories are rare. Where found they consist of three types and occur only in the more massive sandstones. These three types are: (1) Isolated faults, oriented normal to bedding and with a strike at a small angle (less than 20°) to the dip direction (Figure 7a). Displacement along the faults is parallel to bedding (i.e., strike-slip with respect to bedding). (2) Widely spaced normal faults that have strikes parallel to that of bedding. Their dips are always opposite to the dip direction of the bed, and displacements are dip-slip thereby serving to extend the bed parallel to dip. (3) A reverse fault was observed only at the St. Johns locality which makes a high angle to bedding (75°) and has greater than 3 m of displacement. Near the fault surface are soft-sediment small-faults with similar senses of shear and smaller displacements (Figure 7b).

Subsidiary kink-folding. The rocks in the middle structural unit tend to have higher limb dips in the western part of the map area. At one exposure in the west-central map-area a sandstone unit is nearly vertical and is truncated at both top and bottom by nearly horizontal upper and lower structural units (Figure 7c, p. 34). In this unit the beds exhibit a high soft-sediment small-fault density (category 2 geometry) and chevron-folds of continuous bedding units

Figure 7. Soft-sediment features in sandstones near St. Johns, Arizona are (a) Bedding-normal soft-sediment small-faults, (direction of dip is parallel to the pencil), (13 cm in length), (b) Soft-sediment small reverse faults adjacent to larger soft-sediment, reverse fault (hanging wall missing to the left), (c) NW view of 20 m thick deformed middle structural unit, (decollement surfaces are marked with arrows and dotted lines), (d) Closer view of vertical beds in (c) showing details of subsidiary chevron-folding (hammer is 28 cm in length).
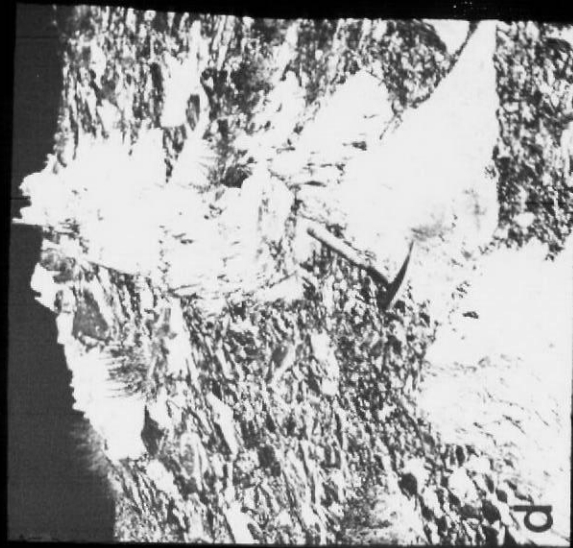
on a small scale (0.15 to 1 m) (Figure 7d, p. 34). This was the only set of beds at the St. Johns locality to display this small-scale subsidiary kink-folding. It is known that during kink-folding, slip occurs on layer contacts such that their normals rotate toward parallelism with the maximum principal stress (Borg and Handin, 1966). The present geometry of subsidiary folds (Figure 7c., p. 34) suggests that the maximum principal stress which produced them is oriented east-west and plunges 30° or more to the west, i.e., oblique to the decollement surfaces. The sense of rotation of these subsidiary folds is always towards the west. The absence of the "conjugate" rotation may suggest the presence of a single sense of shear across the middle structural unit, probably exerted by simultaneous shear motion on both upper and lower decollement surfaces.

Slickensided shear-surfaces. Slickensided shear-surfaces in the claystones are the principal deformational feature present near the decollement surfaces. These shear-surfaces are small curvi-planar discontinuities which show shiny, undulatory slickensides. The density of slickensided shear-surfaces (measured along a line) in the lower unit increases from 50/m at 2 m below the decollement, to approximately 750/m near the upper contact. The nature of the individual shear surface changes from a relatively planar geometry to an anastomosing and undulatory one with proximity to the upper contact. Some of the more planar surfaces are filled with fibrous calcite whose fiber orientation is normal to the fracture surface. These

calcite fracture fillings are 1-3 mm thick (Figure 8a). The anastomosing shear-surfaces near the decollement are highly slickensided, and their fabric is similar to that described by Kliest (1974) for a small-scale argille scagliose. By gross observation the slickensided shear surfaces in the clay tend to have common north-south strike (roughly parallel to the fold-axes and decollement strike).

The upper structural unit is a non-calcareous claystone. Shear-surface intensity decreases more rapidly away from the decollement in the upper structural unit (to 50/m at 0.6 m above the contact). In the upper structural unit the slickensided shear-surfaces show roughly north-south strikes like their counterparts in the lower structural unit. The claystones in both upper and lower structural units have a background density of approximately 10 shear-surfaces per meter where exposed not adjacent to the contacts.

The similarity of character of the sheared claystones, along with the planar nature of both the upper and lower contacts of the middle structural unit; indicates that they are correctly interpreted as decollement horizons. This interpretation is kinematically required at least for the lower contact to explain the discordant relationship of the beds in the middle structural unit to the lower surface. Evidence suggesting simultaneous, oppositely directed senses of shear on both upper and lower decollement surfaces is found in the subsidiary kink-folds of the middle structural unit (discussed earlier).

Figure 8. Soft-sediment deformation features near St. Johns
and Many Farms, Arizona show (a) Slickensided shear-surfaces in
claystone beneath lower decollement at St. Johns, (note that
intensity increases upwards towards the decollement surface), (b)
Category 3 soft-sediment small-faults near Many Farms, (c) Category
3 soft- sediment small-faults down-strike from (b).

Many Farms, Arizona.

General description. The first of the soft-sediment localities
investigated on the western Defiance Uplift is located 8 km east of
the town of Many Farms on Navajo Highway 8. It is reached by an
unpaved Navajo access road with the permission of the Navajo Tribe.
In this area, outcrops which cover an area of approximately 3 km^2,
are as well exposed as those near St. Johns although the drainage is
not as deeply incised. The lithologies are identical to those found
at the St. Johns locality.

Macroscopically, the structures appear as tilted beds varying
in dip from 0 to 35° and striking from east-west to N 15° E. All
dips are to the north or west. Thus, geomorphologically, the area
is a series of similar hogbacks with variable strikes, 40-500 m in
length and spaced 50 to 100 m apart. Unlike the St. Johns area,
there are no exposed complementary fold limbs. Only very thin
bedded units in this locality demonstrate noticeable bending; massive
units, as at St. Johns, are noticeably less faulted. No decollement
surfaces such as those found at the St. Johns locality could be
identified here, however the base of the inclined units is not
exposed, so the possible existence of a lower decollement cannot be
excluded.

Soft-sediment small-faults. The most obvious deformation features are soft-sediment small faults, identical in morphology to those described at the St. Johns locality, and exhibiting the geometry of both category 1 and category 2 (Figure 5a, b, p. 29) discussed earlier. One outcrop contains an extensive (10 m x 2 m) exposure of soft-sediment small-faults of category 3 (Figure 5c, p. 29). The acute angle between the strikes of the two sets of conjugate faults bisected by the dip direction is slightly higher (up to 34°) than that for the conjugate shears bisected by the strike direction (approx. 20°). The additional planes in category 3 also show both normal and reverse senses of slip (consistantly only one or the other at any one place on the outcrop), and are in orthorhombic symmetry with respect to the bedding (Figure 8b and c, p. 38).

Careful measurements were made of fault orientations and senses of slip in hand specimens collected from all of the soft-sediment localities. With all data rotated to a common strike, the arrays of small faults have conspicuous orthorhombic symmetry (Figure 9a, b). Not all faults are present in all samples, however all samples show at least 3 fault orientations (Figure 9). The reason for the complexity of the fault systems is not apparent at any of the soft-sediment localities.

Agathla Peak, Arizona.

General description. The third locality investigated is 10 km northeast of Kayenta, Arizona near U.S. Highway 63. Its exact location

Figure 9. Equal area projections of soft-sediment small-fault orientations measured in hand specimens with data rotated to a common strike. The plane of projection is parallel to bedding with strike and dip directions as shown. (a) 45 normal faults from 8 hand specimens. (b) 9 reverse faults from 2 hand specimens.

a.

NORMAL FAULTS

b.

REVERSE FAULTS
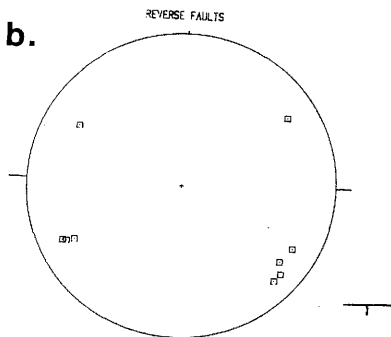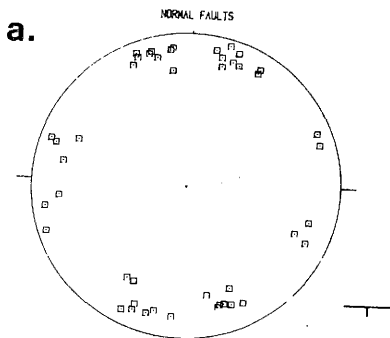
is immediately to the northwest of Agathla Peak on the southwest part of the Monument Upwarp and northwest of the Defiance Plateau. The rocks deformed at this locality are also very similar to those observed at St. Johns.

Linear hogbacks, truncated units, and other features similar to those at St. Johns are developed but to a lesser degree of intensity. Beds are gently inclined and generally show little bending. Opposed limbs of folds are present (hinges being totally or partially eroded) with lower dips than those at St. Johns. There is no strong evidence to suggest the presence of a lower decollement zone at this locality, as truncating surfaces are not traceable for large distances.

Soft-sediment small-faults. At this locality, the rocks show soft-sediment small faults of similar character to those discussed above. One hogback contains excellent exposures displaying the three dimensional geometry of the category 2 small faults (Figure 10a). A vertical face parallel to dip reveals the cross-sectional orientations (apparent dip) and the magnitudes of slip on each fault of a category 2 array (Figure 10b). The magnitude of displacement, apparent angle to bedding, and the distance between faults along the line of the traverse were measured along this outcrop. By determining the extension parallel to bedding due to each fault[1], summing them and subtracting that sum from the measured traverse length, a

---

[1] The extension parallel to bedding as a result of displacement along each fault is the product of the magnitude of the displacement and the cosine of the apparent angle it makes with the bedding.

Figure 10. Soft-sediment small-faults in sandstones near Agatha Peak Arizona. Shown are (a) Bedding plane exposure of category 2 small faults (13 cm long pencil is parallel to strike, dip is toward the bottom of the photo), (b) dip section of exposed category 2 faults that were measured to determine extensional strain in the dip direction (hammer is 28 cm long), (c) low-angle fault plane and conjugate in lower layer of exposure. in (d), (d) outcrop showing variation from high-angle normal to low-angle normal faults from top to bottom of sandstone exposure.
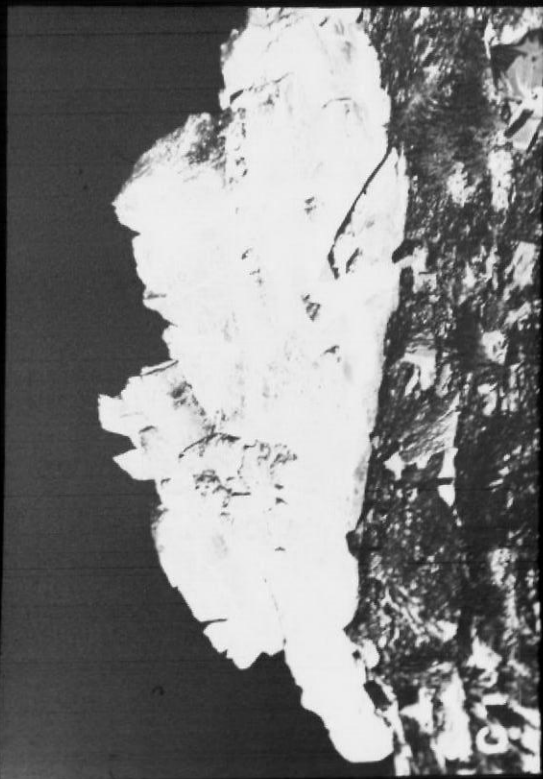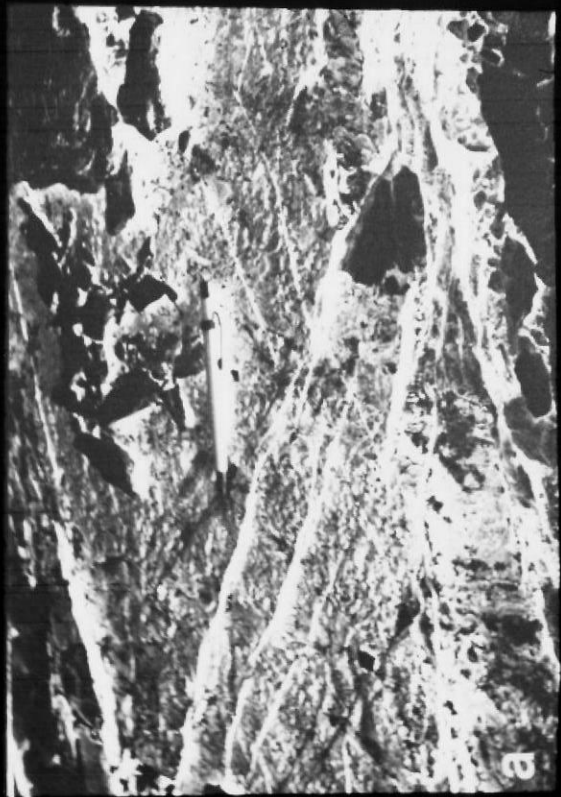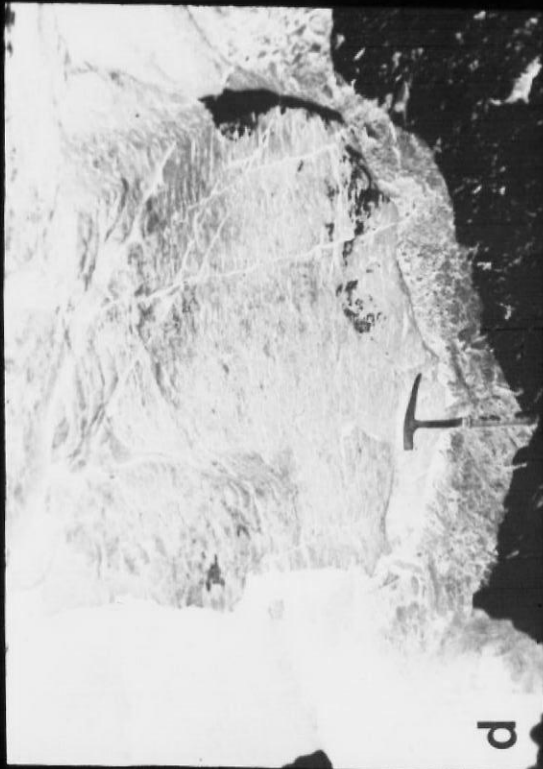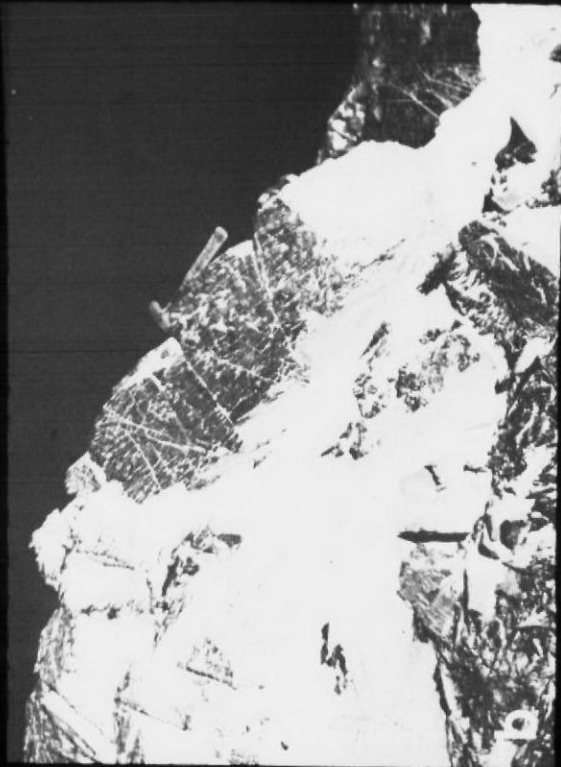
close approximation is made of the pre-faulting length of the traverse line. Because the orientation of bedding is a constant reference direction both pre- and post-faulting, the measurement of a traverse parallel to bedding eliminates the need for corrections due to possible rotation of the traverse reference line. Given the initial and final traverse line length, the total elongation due to faulting is calculated to be 6.8% in the dip direction (Table 1). This was the only locality where a quantitative analysis of deformation due to soft-sediment processes was possible.

In this same sandstone unit the fault density and relative inclination to bedding decrease toward its base. The fault displacement in its lower portion is extensional with respect to bedding with displacements along low-angle faults which dip away from the direction of bedding dip (a characteristic also noted at St. Johns). A fault set with another orientation was found in the lower massive rocks. These occur at a high angle to bedding, and may be conjugate to the low-angle faults (Figure 10c, p. 46). They show no visible off-set, however variations in fault types and density with position on the outcrop can be seen in Figure 10d, (p. 46.) The locations of these faults indicate that flexural-slip on fold-flank bedding could be responsible for the reorientation of stresses and the consequent low-angle normal-fault conjugate-set in the basal layer. The fault geometry in this outcrop, as well as the conspicuous bedding planes which separate the thin and massive units are very similar to the

Table 1. Length changes due to soft-sediment faults

Fault No.	Distance Along Trav (mm).	Displacement (mm).	Fault Dip (° to west).	Angle to Bedding (Traverse) (°).	Elongation of bedding due to fault.(mm)
1	0	3.0	20	69	1.1
2	15	5.0	12	61	2.4
3	41	10.0	25	74	2.8
4	61	3.0	65	66	1.3
5	85	10.0	67	64	4.4
6	91	2.5	48	83	.3
7	124	1.0	66	65	.4
8	174	2.0	14	63	.9
9	219	10.0	32	81	1.6
10	306	42.0	29	78	8.7
11	411	15.0	69	62	7.0
12	466	7.0	55	76	1.7
13	496	9.0	53	78	1.9
14	543	5.0	57	74	1.4
15	588	38.0	17	66	15.5
16	768	5.0	21	70	1.7
17	883	7.0	68	63	3.2

Final Trav. =883 mm
    Length

Elongation = 56.3 mm
(Length Change)

INITIAL TRAVERSE LENGTH = FINAL TRAVERSE LENGTH (ELONGATION)
                        = 883 - 56.3
                          826.70

% Elongation in Dip Direction = (56.3/826.7) x 100%
                              = 6.8%

the fault and layer relationships of a layered clay model which will
be discussed in the chapter "Model Studies."

Chinle Area, Arizona.

An area 2 km south of the town of Chinle Arizona (west central
part of the Defiance Plateau) is dominated by several ridges spaced
roughly 0.5 km apart striking an average of N 70° E. One of the
more prominent ridges was examined for this study. It is capped by
a lime-pebble conglomerate (lpc) folded in the same style as the
sandstones described previously. The lpc is 1 to 1.5 m thick, and
is underlain by a massive red claystone which contains diffuse gray
massive bedding. It is composed of 0.2 to 4 cm pisoliths, micritic
limestone pebbles, and some coarse quartz grains.

A chevron fold is developed in the conglomerate. The erosional
remnant of this fold is a very sharp syncline with the only notice-
able bending of the limbs occurring as a slight undulation along
strike (Figure 11a). The extremely sharp synclinal hinge is broken
so that there is a discontinuity along the axial plane. A unique
feature at this locality is that all of the claystone exposed beneath
the lpc mimics the orientation of the lpc beds, indicating little
detachment proximal to the lpc horizon. The lpc is relatively unde-
formed between hinges, however it contains a few widely-spaced open
fractures that are normal to bedding. Some of the fractures are
parallel and some are perpendicular to the outcrop face. These frac-
tures are similar to the open fractures at the St. Johns locality,

Figure 11. Soft-sediment features on the West and East flanks of the Defiance Plateau. Shown are (a) West view of sharp synclinal fold in lime-pebble conglomerate near Chinle, Arizona, (hinge is marked by arrow; automobile in ravine is approximately 4.5 m in length), (b) sharp recumbant fold in stream exposure near Nazlini, Arizona, (c) vertical middle structural unit beds (below) in decollement contact with a lime-pebble conglomerate near Ft. Defiance, Arizona (note thin layer of smeared-out sand developed between the two), (d) oblique view of striated decollement surface sandstones of the middle structural unit near Ft. Defiance.
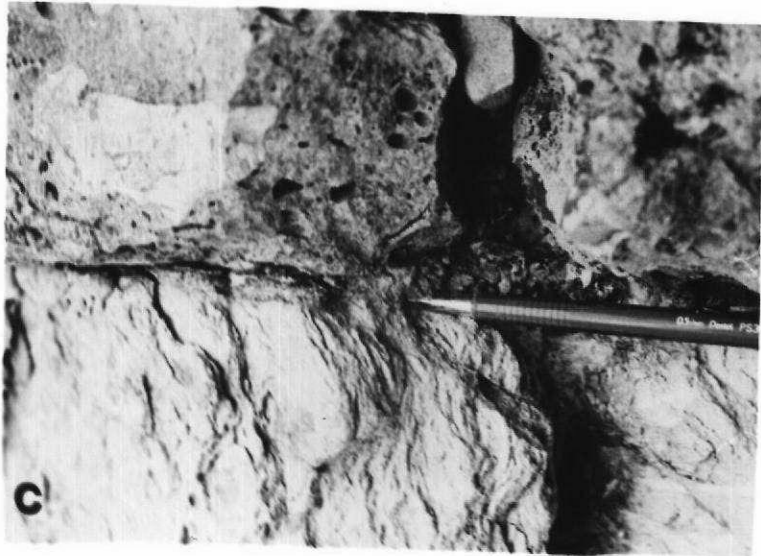
and are probably the product of exposure-induced stress-relief.
Interpenetration (pressure solution?) is obvious on some of the
larger limestone clasts, however the conglomerate is not well
cemented and is very friable.

Nazlini Area, Arizona.

    In an area 7 km northwest of Nazlini, Arizona, in a small
ravine, a small recumbent fold was discovered whose axis is horizon-
tal and trends N 5° E (Figure 11b, p. 52). Much of the overturned
limb has been truncated. It demonstrates some of the mechanisms
which operate during folding under soft-sediment conditions. The
core of the fold is dominated by sandstones which have a higher clay
content on individual bedding horizons than those along the outer
fiber of the fold. The interior layers of the fold are dominated by
flexural-slip folding, while the outside layers of the fold are
dominated by soft-sediment faulting (category 2). The latter reaches
a density of 100 faults/m in the hinge region. The overall result
is that the outside unit of the fold thins approximately 50% whereas
the interior of the fold actually thickens slightly (10% due to some
flexural flow). In addition, the presence of a neutral-fiber
(extention to compression transition) is suggested by the presence
of small crenulated layers in the innermost compressed hinge and of
the extensional fault system (category 2) in the outer units of the
fold.

Hard-rock Deformation.

Two localities of Laramide hard-rock deformation on the east
flank of the East Defiance Monocline were studied and mapped in
detail. These areas were chosen for examination because (1) the
sandstones in the Petrified Forest Member are well exposed and (2)
the structures can be readily linked to the larger Laramide features.
The Petrified Forest Member sandstones differ from the Monitor Butte
Member sandstones observed in the soft-sediment deformation locali-
ties as follows:

> (1) The Petrified Forest sandstones tend to be fine to medium
> grained, i.e., slightly coarser than those lower in the section
> (Monitor Butte Member).

> (2) The Petrified Forest sandstones generally are more mas-
> sively bedded, and show more large-scale cross-bedding, and
> ripple-lamination than the Monitor Butte Member.

> (3) Petrified Forest sandstones exhibit more thick individual
> sand units (3-4 m) separated by claystones of variable thick-
> ness, whereas Monitor Butte sandstones are more commonly
> thinner-bedded (0.5-1.0 m), with intercalated claystones.

The sandstones in the Petrified Forest Member also bear the
following important similarities to those in the Monitor Butte
Member, namely:

> (1) Both members share similar source areas with only a slight
> temporal difference. Consequently, the detrital as well as the
> argillaceous components are very similar in both members,
> (Table 2).

Table 2. Compositional and textural characteristics of the Lower Chinle Members.

	Quartz	Na-Feldspar	K-Feldspar	Volcanic det.	Calcite	Average Grainsize
Petrified Forest Member	1-80	0-36	0-25	0-95	0-68	Very fine to coarse
Monitor Butte Member	5-85	0-22	0-15	0-84	0-70	Very fine to granules

From: Stewart and others (1972).

(2) The gross stratigraphic and consequent structural positions are equivalent (only about 60 m of section separate the two groups of sandstones).

Ft. Defiance Area, Arizona.

General description. The first hard-rock deformation locality consists of approximately 20 km^2, centered 3 km Northeast of Ft. Defiance, Arizona (Figure 12, pocket). The Monitor Butte Sandstones are not exposed here and may be faulted out in the northern part of the mapped area. Petrified Forest Sandstones are 30 to 40 m thick where undisturbed.

The deformation in this locality (Figure 12, pocket) is dominated by a branching shallowly eastward-dipping thrust fault

that apparently becomes a bedding plane detachment in the Chinle Formation in the subsurface to the east. The fault trends roughly NNE and cuts obliquely through all members of the Chinle along strike (Figure 12, pocket). In the northern mapped area (Figure 12), east of the thrust fault, are multiple ridges of the Sonsella Sandstone which dip 10 to 50° east and strike from N 20° W to north-south. The multiple sandstone ridges are the direct result of imbrication above the major fault, as evidenced by repetition of distinct lithologic sequences. Folds which plunge and die along strike and exhibit wave lengths of 25 to 300 m also occur in this zone. Their steeper flanks face west, and often one limb is poorly or not exposed. The hinge regions of these folds are typically very tight (chevron). Fold limbs are rarely noticebly bent. Bedding units in the area east of the thrust fault are usually traceable for 200 to 500 m before plunging below the surface or being truncated at a low-angle by another fault branch. Many of the characters of the deformation in this area are similar to those of the soft-sediment localities, however outcrops investigated in this locality, do not exhibit any soft-sediment small-faults which are known to be abundant in all of the soft-sediment localities.

Thickness changes. A section was measured in two parts starting just south of the mapped area, west of the fault; and ending in the eastern map area above the faulted section. This section is used to

determine Chinle thickness changes excluding that due to faulting. Compared to average undisturbed thickness at this location the unfaulted section shows a range of 4.2% thinning to 72.6% thickening (Table 3). In addition, there is appreciable thickening of the section due to fault-imbrication of the Sonsella Sandstone. A conservative estimate of fault-dominated thickening is 360%. This estimate is based on a dip of 10° and a surface exposure width of 620 m. It yields an estimated thickness of the sandstone section of 108 m (normal thickness: 30 m).

Thus, the thickness changes in the Petrified Forest Member are accomodated by two mechanisms: (1) macroscopically homogeneous flow probably by displacement on closely spaced shear surfaces found in the claystones (0 to 72% thickening), and (2) faulting imbrication of the sandstone units which are resistant to homogeneous flow (locally up to 360% thickening). An estimate of thickening of the entire Chinle Formation due to both mechanisms in the map area is 72%.

Fractures. Open fractures are the most evident of all macroscopic deformational features in outcrop in this area. They are ubiquitous but show variation in local intensities (Figure 13, a, b). They are all normal to bedding.

The open nature of the fractures suggests that they are the loci of failure due to loss of cohesion, and they formed in an indurated, cemented rock, capable of maintaining an open fracture. Their local

Table 3. Thickness changes measured at the Ft. Defiance locality.

	Normal[1] thickness (m).	Measured thickness (m).	% Thickening.
Owl Rock Member	55 m	57.0 m	+ 3.6%
Upper Petrified Forest Member	200 m	345.2 m	+72.6%
Sonsella Sandstone Bed	30 m	28.8 m	− 4.2%
Lower Petrified Forest Member + Monitor Butte Member	107 m	141.0 m*	+31.8%

(*)partially buried by alluvium—may be faulted.

(1) from Stewart and others (1972) and Reppening and others (1969).

Figure 13. Macroscopic hard-rock features 3 km northeast of
Ft. Defiance show (a) and (b), open hard-rock fractures, (c) hard-
rock small-fault in medium-grained sandstone. The view is down
dip. Pencil is parallel to bedding (Note that the faults are more
resistant-weathering than the host-rock.)
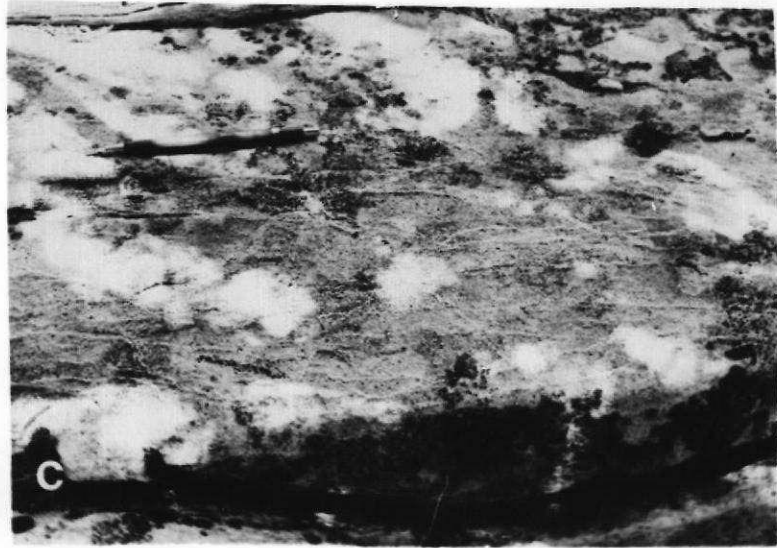
intensity (up to 30 fractures/m) suggests that they are the result of a deformational episode whose intensity could only be attributed to the hard-rock category. None of the soft-rock localities exhibit an intensity of fractures as those found here.

Stearns (1968) postulates that the origin of the geometry of natural fractures, such as those investigated here is related directly to bending stress produced by folding. Norris (1967) reached similar conclusions. In contrast, Reches (1977) concluded that the fractures on two monoclinal folds in Israel resulted from a regional stress field. He notes that the strikes of individual sets do not follow the strike-variations of the monoclines.

In order to analyze the significance of the fabric of fractures in the Ft. Defiance area, all fracture strikes measured at a particular station are plotted with bedding rotated to horizontal. Rose diagrams of fracture strikes from individual stations are shown in Figure 12, (pocket). If bending stresses from localized folds are responsible for the observed fractures, then superposition of data from all stations rotated to a common strike should reveal a strong pattern. It is reasoned that fractures generated by bending in folds will be geometrically related to one of two principal stress directions, (maximum or mininum). Bedding strike (bending axis) should be perpendicular to that stress direction (i.e., fractures on two folds of varying orientation should superimpose when their strikes are rotated to parallelism). These patterns are not reflected strongly in the data (Figure 14a). If a regional, homogeneous-stress field is primarily responsible for the fracture
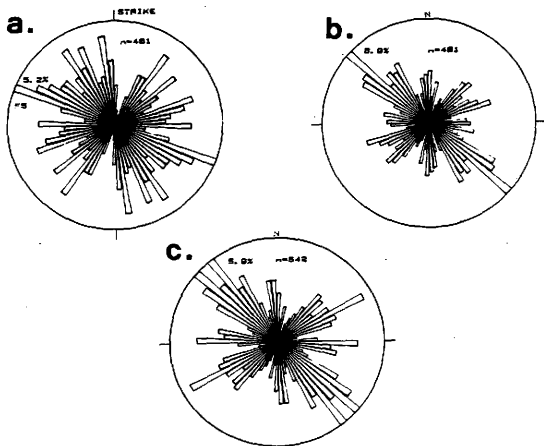
Figure 14. Composite rose diagrams of hard-rock fracture strikes. The plots show a) Ft. Defiance locality hard-rock fractures with corresponding bedding rotated to a common strike, (average strike is oriented north-south, as shown, (b) same data as (a), with bedding rotated to horizontal around its strike but otherwise left in field orientation (no rotation of bedding-strikes to common direction). (c) All fracture strikes from East Defiance Monocline, with bedding rotated to horizontal (no rotation of bedding-strikes).

orientations, then the same data, superimposed with unrotated strikes, should yield a strong pattern (Figure 14b). The pattern in Figure 14b (p. 63) is slightly stronger than that in 14a suggesting the influence of a regional stress field. Figure 14c, (p. 63) shows the fracture strike orientations from the Ft. Defiance area combined with those from as much as 12 km north or 50 km south of that area. The pattern in Figure 14b (p. 63) appears to be reinforced in Figure 14c (p. 63) despite the large sampling area, again suggesting a regional consistency of the stress field which produced them. The presence of locally high densities of these fractures in areas of tectonic folding and faulting, however, suggests that their intensity is localized by the folding and faulting events themselves, even though their orientations may possibly be linked to a more regional stress system.

Hard-rock small-faults. In addition to fractures, hard-rock small-faults were observed in medium grained sandstones. Hard-rock small-faults are small displacement-discontinuities, generally found in deformed porous-sandstones. They were described and analyzed by Aydin (1978) and Jamison (1979). They consist of sub-planar fault-zones of crushed and comminuted sand grains approximately 1 mm wide. Their individual shear-displacement is usually less than 2 cm, with greater displacement often accommodated by anastomosing groups of individual bands. The conditions of formation attributed to these faults by both Jamison (1979) and Aydin (1978) fall into the hard-rock category, defined here. This is because the grain-

crushing associated with the hard-rock small-fault formation requires both lithification and high stress differences. Hard-rock small-faults are therefore considered accurate markers of hard-rock deformation.

The hard-rock small-faults immediately above one of the branching thrust-faults in the Ft. Defiance hard-rock locality tend to anastomose in strike section while remaining parallel to bedding dip (Figure 13 c, p. 61). Slickensided surfaces broken from near bedding-parallel hard-rock small-faults show dip-slip displacement of N 85° E. Although the hard-rock small-faults' exact relationship to the stress-field which produced them has not been fully demonstrated, the fact that slickenside direction is roughly east-west is indicative of an east-west striking vertical plane which contains the maximum and minimum stress directions. This conclusion is reinforced in the chapter "Laboratory Studies".

Lupton Area, Arizona.

General description. The second locality of hard-rock deformation is an area of approximately 35 km^2 centered 3.5 km NNW of Lupton, Arizona (Figure 15, pocket). The structure in this area is a moderate to steeply-dipping, faulted moncline with varying strike. A prominent feature is a west-dipping reverse fault with 0 to 125 m of stratigraphic throw that cuts the monocline just to the east of the map trace of the upper hinge. At one exposure the fault (dipping 28° W, striking north-south) puts Moenkopi Formation on

slightly overturned Petrified Forest Member sandstones. This relationship indicates a stratigraphic throw of about 125 m. The Sandstone beds in the area dip from 45° E to 70° W (overturned) and strike between N 52° W and N 33° W.

Thickness changes. Three Chinle sections were measured in as many strike normal traverses across the monocline (Figure 14, p. 60). In all three sections the Monitor Butte member is faulted out and was not measured. The Chinle members measured above the faulted section show a 7 to 72% thickening (Table 4), compared to average undisturbed thickness values in this locality from Stewart and others (1972) and Reppening and others (1969).

The thickened section here is not in conflict with the work of Jamison (1979) and Vaughn (1976) for similar structures who show a general thinning of clastic units over the upper hinge of the mono-cline. The apparent contradiction can be resolved by considering the cross section through the central postion of the Lupton area (Figure 16). The first two sections were measured at a horizon represented by line A in Figure 16. The third section was measured on a horizon schematically represented by line B. All of these sections are thickened. If the section were measured higher on the structure, however, such as at horizon C, it would be attenuated. In general, below the "inflection point" of the structure, the units most susceptible to thickness changes (Chinle Formation) will be thickened whereas above the "inflection", they will be thinned.

Table 4. Thickness changes measured at the Lupton locality.

Member Name.	Section number.	Normal[1] thickness.	Measured thickness.	Percentage thickness change.
Owl-Rock Member 72.0%	1	40 m	61.5 m	53.8%
	2	40 m	62.0 m	55.0%
	3	40 m	69.0 m	72.0%
Upper Petrified Forest Member 72.0%	1	162 m	233.1 m	43.8%
	2	162 m	173.4 m	7.0%
	3	162 m	278.7 m	72.0%
Sonsella Sandstone Bed 55.4%	1	56 m	61.6 m	10.0%
	2	56 m	67.8 m	21.1%
	3	56 m	87.0 m	55.4%
Lower Petrified Forest Member	1			
	2	FAULTED	OUT	
	3			
Monitor Butte Member	1			
	2	FAULTED	OUT	
	3			

(1) From Stewart and others (1972) and Reppening and others, (1969)

Figure 16. Identical controlled cross-section through central Lupton-locality showing variation in thickness of the Chinle Formation. Dashed lines are lines of equal thickening, indicated in percent. Vertical and horizontal scales are equal. Sections are drawn along line of section in Figure 15 (p. 67).

WEST   EAST

ELEVATION
ABOVE SEA LEVEL
FEET(METERS)

TR-J

TRc

TRm

Pdc

Ps

PC

K

8000(2461)

6000(1846)

6000(1846)

TR-J

TRc

Pdc-Ps

PC

C

B

A

8000(2461)

6000(1846)

6000(1846)

99
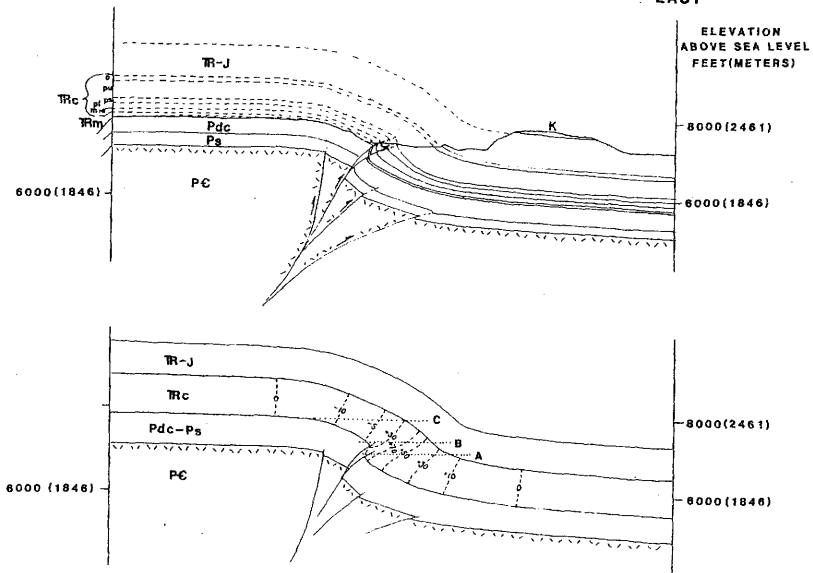
The thickening mechanism in the Lupton area is one of homogeneous flow. All members measured above the thrust-faulted section apparently thicken without large-scale faulting (Table 4 p. 64). Cataclastic-flow of the clay-rich members is proposed as the major mechanism of thickening. Macroscopically this flow appears to be accomplished by small displacements on homogeneously-spaced slickensided shear-surfaces in the claystones. These surfaces are morphologically similar to those observed in high concentrations at decollement surfaces in the claystones at the soft-sediment localities. Similar features also have been described in association with the Lewis thrust in Northwestern Montana where there is no doubt that they are attributable to hard-rock style deformation and apparently must accommodate large tectonic strains (Wilson, 1970).

Fractures. The sandstones in the Chinle of the Lupton area show high concentrations of open fractures (up to 30 fractures/m) identical in morphology to those described earlier. Fractures from three outcrops, rotated to horizontal along strike, show two major trends; one is nearly east-west, the other is N 65° E (Figure 15, pocket).

Localities Exhibiting Soft-Sediment and Hard-Rock Deformational Features

Two localities dominated by soft-sediment deformational features located on the East Defiance Monocline contain slight overprinting of hard-rock deformation. In one case, this overprinting is documented by the presence of hard-rock open fractures. In the other

case it is merely inferred by the structural position of the locality
on the monocline. In the latter, the interpretation of overprinting
is borne out in the succeeding chapter "Laboratory Observations."
The lithologies involved in these structures are identical to those
observed at the St. Johns locality (Monitor Butte Member).

Ft. Defiance, Arizona.

General description. The first overprinted locality is located .5 km
south of Ft. Defiance, Arizona, on the shallowly eastward-dipping
flank of the East Defiance Monocline. The major structural features
at this locality are quite similar to those found near St. Johns,
i.e., they are soft-sediment features. The exposure consists of 3
structural units, lower, middle, and upper; equivalent in relative
position to their counter-parts at the St. Johns locality. The
structure is an asymmetric east-west trending anticline which has a
southern vertical or near vertical limb striking east-west, and a
northern limb dipping 23° N and striking N 30° E. The fold axis
trends N 85° E with a plunge of approximately 20° E. The fold is
truncated at the top and bottom by planar decollements which define
the contacts of the middle structural unit with the non-folded upper
and lower structural units. The thickness of the middle structural
unit varies from 21 to 33 m. The lower decollement surface is
clearly defined by the sharp boundary of the green, calcareous,
micaceous sandstone and claystone (middle structural unit) with the
red, non-calcareous claystone of the lower structural unit. The

upper contact also is defined by a sharp boundary with a lime-pebble conglomerate/medium-grained massive sandstone (upper structural unit) in angular disconformity with the rocks of the middle structural unit.

Decollement surfaces. The fabric of the lower unit claystones near the lower decollement is quite similar to the fabric of the claystones described at the St. Johns locality. It consists of a small-scale argille scagliose with slickensided shear-surface density exceeding 400/m in the vicinity of the decollement surface, and grading to 15/m at 2 m below the decollement. The upper structural unit differs from that at St. Johns in that it is composed fine to medium-grained, quartz cemented massive sandstones, with localized lime-pebble conglomerates, in immediate decollement contact with sandstones and claystones of the middle structural unit. The continuity of the bedding in the middle structural unit is maintained to within 1 cm of this contact (decollement) making for a very sharp boundary (Figure 11c, p. 50). In some places along the exposure, a thin layer of fine-to medium-grained, calcite-cemented sandstone is found at this decollement surface between the middle and upper structural units. Where the sandstone of upper structural unit has been removed by erosion, a shiny manganese-oxide coated, striated surface of the sandstone in the middle structural unit is exposed (Figure 11d, p. 50). This surface is not parallel to but is within 10° of the dip of middle unit the sandstones on which it is formed. The only place where this surface is exposed is in the hinge region

of the truncated anticline. Soft—sediment small—faults (category 1) cut the surface perpendicular to the striations (Figure 17a). It is probable, based on the interrelationship of the striae and the small faults that both the striae and the small faults formed simultan—eously. The consistency of both the direction and morphology of the striae implies that they were formed by sliding of the upper structural unit over the middle structural unit while bending of the beds in the lower structural unit was responsible for simultaneously producing the soft—sediment small—faults. The direction of asymmetry of the anticline and the direction of striation orientation suggest a S 5° E slip direction along the surface.

Fractures. Open fractures (3-4 fractures/m) are present in the upper unit. The fractures are normal to bedding of the upper unit, but exhibit a variety of strikes in any one outcrop. Their moderate density, and their open, bedding—normal characteristics suggest they are hard—rock features due to Laramide deformation. The strikes of the fractures in the upper structural unit, with bedding rotated to horizontal are shown in Figure 18.

Navajo Roadcut, Arizona.

The second locality dominated by the soft—sediment style of deformation with slight tectonic overprinting is located 5.2 km west of the town of Navajo, Arizona, on a Navajo service road. The expo—sure is a road—cut at the topographic crest of the eastern margin of

Figure 17. Soft-sediment features on the east flank of the
Defiance Monocline. Shown are (a) soft-sediment faults of category
1 cutting decollement surface of the middle structural unit near Ft.
Defiance, (b) panoramic view of soft-sediment deformation in roadcut
west of Navajo, Arizona. Carryall at left is 2.5 m wide, (c) rare
soft-sediment small faults which are normal to bedding in roadcut
shown in (b) (note that displacement is strike-parallel).
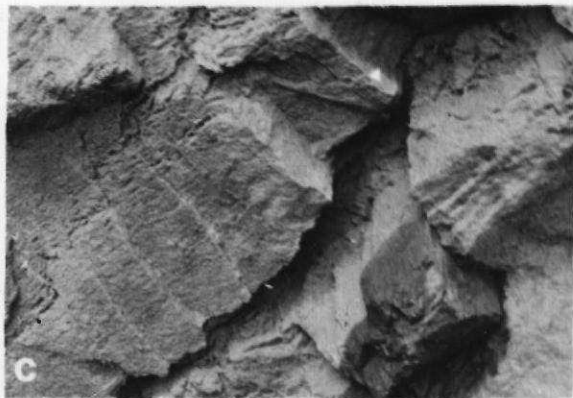
Figure 18. Map of soft-sediment deformation locality south of Ft. Defiance, Arizona. Rose diagrams show strikes of bedding-normal hard-rock fractures at this locality and their location on the structure. For legend see Figure 4 (p. 25).
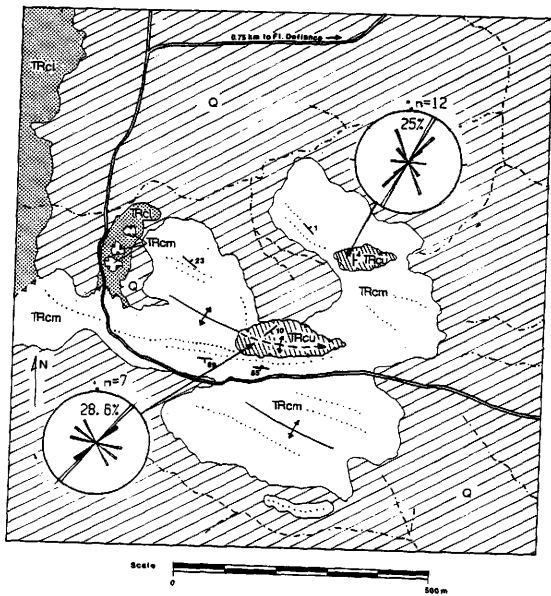
the East Defiance Monocline, slightly closer to the upper hinge than the locality south of Ft. Defiance.

The outcrop consists of beds dipping 50° W to near vertical and striking nearly north-south (Figure 17b, p. 72). This strike is 90° from that at Ft. Defiance. Mud-crack fillings occur in the western part of the roadcut that indicate some of the beds are overturned. The dipping beds in this outcrop are truncated and overlain by similar lithologies which dip slightly (approximately 5°) to the East. There is a small thrust fault which dips west and cuts the section in the western part of the roadcut. This fault also cuts some of the horizontal beds above the truncation surface.

The inclined beds show features similar to those found at the St. Johns locality and the other soft-sediment localities. These features are: (1) soft-sediment small-faults (category 2), and (2) slickensided shear-surfaces in layers of more clay-rich material between sandstone beds. The clays show only a slight increase in intensity of slickensided shear-surfaces near the horizontal beds at the top of the exposure. This is in notable contrast to similar surfaces (decollements) at other localities where slickensided shear-surfaces are intensely developed. The more undulatory nature of this surface suggests that it was not the locus of any appreciable sliding. Unlike its counter part at St. Johns and Ft. Defiance, this surface probably is as an angular disconformity. The thrust-fault, in the western part of the roadcut, which shows no evidence for Laramide origin (i.e., open fractures), occurred after the deposition of the horizontal beds, suggesting a scenario of ongoing

deformation, erosion, and deposition of unstable sediments in Triassic time. Other unique features found at this locality are soft-sediment small-faults oriented nearly normal to bedding and parallel to strike (Figure 17c, p. 72), that have shear displacements parallel to bedding plane. In addition some small faults occur that strike parallel to the strike of bedding, dip at a low angle to and opposite to the dip of bedding, and that show normal-fault displacement relative to bedding.

Open fractures are rare at this locality. Hard-rock overprinting at this locality is inferred in the field from it's position on the East Defiance Monocline. Substantiation of overprinting of hard-rock deformation at this locality is given in the chapter "Laboratory Observations."

Summary of Deformation Features from Field Observation

Soft-sediment features. Macroscopic soft-sediment deformation features which are unique to areas which have no Laramide over-printing are:

(1) Soft-sediment small-faults. These faults offset the bedding at high angles and weather preferentially relative to the host-rock. They are developed in beds distant from any known Laramide structures, and therefore are clear-cut macroscopic indicators of soft-sediment deformation. Their geometry (orthorhombic symmetry), morphology and abundance are unique in the sandstones which could only

have deformed under soft-sediment conditions (as defined
on p. 10). Because the features are present in great
abundance in all areas of soft-sediment deformation inves-
tigated they are considered common enough to be useful
generally to recognize soft-rock deformation of sandstones
and claystones lithologies.

Hard-rock features. Macroscopic features unique to rocks affected
by hard-rock deformation are as follows:

(1) Open fractures oriented normal to bedding are ubiquitous
indicators of this type of deformation, owing to their
locally intense ordered development only in localities
which are known to have been involved in Laramide deforma-
tion. Their locally intense, development and distinctive
open appearance make them a useful macroscopic indicator
of hard-rock deformation.

(2) Hard-rock small-faults, are found only in hard-rock
deformation localities but are restricted to high-strain
areas such as near major faults. In the study area they
are typically oriented near-parallel to bedding and show
reverse weathering and lighter color due to finer-grained
and comminuted material in the zone.

Ambiguous features. The largest group of structural features ident-
ified in the field, are of ambiguous character, i.e., non-specific
for either soft-sediment of hard-rock deformation. Because so many

of the macroscopic features are ambiguous further microscopic distinction is desirable. (The following chapter, successfully establishes additional microscopic criteria.) The macroscopic features present in localities with either type of deformation are as follows:

(1) Chevron-type folds are present on scales from 1 to 300 m in wavelength in all areas studied. They show little or no limb bending and have poorly exposed hinge zones.

(2) Decollement surfaces, thrust-faults and truncations are present in areas containing either style of deformation. In addition, angular unconformities occur in the soft-sediment areas and are difficult to distinguish from structural truncations.

(3) Plunging and dying fold character are present in all areas. Folds, as well as individual limbs are rarely tracable for large distances in any of the areas due to plunging-out as well as due to (2).

(4) Slickensided shear-surfaces in claystones. These small surfaces of discontinuity are present in abundance in both soft-sediment and hard-rock localities and apparently play an important role in both styles of deformation as evidenced by soft-sediment decollements and Laramide-induced homogeneous thickness-changes, yet they are indistinguishable in appearance regardless of deformational regime.

CHAPTER III

LABORATORY OBSERVATIONS

Introduction.

Macroscopic observations discussed in the previous chapter have established field criteria for recognizing soft-sediment versus hard-rock deformation. Due to the abundance of ambiguous features present at the macroscopic scale of observation, and as a consequence of the current understanding of deformation mechanisms and environments at the microscopic scale, microscopic observation was deemed a useful, if not vital complement to the field observations of these deformed rocks.

Sample preparation.

Oriented sandstone specimens from the 8 localities described earlier were collected for microscopic analysis. The following procedure was used to prepare sandstone samples for analysis:

(1) 2 cm-diameter cores were drilled from oriented specimens.

(2) These cores were impregnated with blue-dyed low-viscosity epoxy under a vacuum for 20 minutes followed by pressure (20 MPa) applied by argon gas in a pressure chamber (2 hours).

(3) Thin sections were made along planes (i) normal to bedding and parallel to dip; (ii) normal to bedding parallel to

strike; and (iii) parallel to bedding (for some samples only (i) and (ii) were cut).

Claystone samples designated for observation with SEM were prepared in the following manner.

(1) The oriented samples were cleaved along planes of specific orientation so as not to disturb the natural fabric.

(2) This chip was trimmed to roughly 1 cm x 1 cm x .5 cm and mounted cleaved-surface up on oriented aluminum stubs.

(3) Analysis of density changes in these samples indicated that special freeze drying was not necessary to preserve original fabric. As a result simple oven-drying for 12 hours at 45°C was used on the mounted samples.

(4) The dry samples were coated with approximately 100 angstroms of gold-palladium alloy in a standard vacuum-evaporator and observed immediately thereafter.

Sandstone Petrography.

All of the sandstones observed in thin section are lithic arenites. Average grain sizes ranged from .11 to .46 mm. The principal components of these lithic-arenites are (1) quartz (22 - 85%), (2) chert (5 - 18%), (3) volcanic lithics (5 - 30%), (4) devitrified or partially devitrified volcanic lithics (4 - 60%), (5) calcite (usually as a cement) (0 - 63%), and (6) micas and clays or oxides as grain coatings and pore fillings (0 - 10%). Heavy minerals are rare.

Porosities range from 0 - 26%, averaging 17%. One sandstone

sample showed detrital grains "floating" in up to 80% devitrified
volcanic detritus and clay. Two additional samples had a similar
relationship of "floating" grains in 60% calcite-spar cement. These
three samples were exceptional and are identified with stars in the
graphs below because of their possible exceptional deformational
character.

Two sections were cut from a sample of the lime-pebble con-
glomerate collected near Chinle, Arizona. This sample contains (1)
78% large fine-grained limestone clasts (averaging 6.4mm), (2) 7%
other lithic clasts, (3) 12% calcite cement and, (4) 3% other clays
and oxides.

Soft-sediment deformation.

Soft-sediment small-faults.

Samples containing the macroscopic soft-sediment small-faults
were sectioned perpendicular to the fault-planes for analysis. All
faults showed the following characteristics (Figure 19):

(1) Deformation manifested by disturbed packing is restricted
    to a zone less than 2 mm wide.

(2) No grain-size reduction due to grain crushing or fracturing
    occurs in the zone.

(3) Higher percentages of clay and calcite cement as well as
    more disordered packing are obvious features of the fault-
    zone.

(4) If quartz overgrowths are present in the host-rock, they

Figure 19. Characters of soft-sediment small faults in thin
section are shown by a) bedding-plane (horizontal) is cut by a soft-
sediment small-fault (note change in packing and increased clay
pore-filling in fault zone) b) close up of fault zone shows details
of soft-sediment small-fault in (a) (note no grain-size reduction,
the open packing and the greater abundance of matrix). Scale bar is
3 mm in (a) and .75 mm in (b). Plane polarized light.
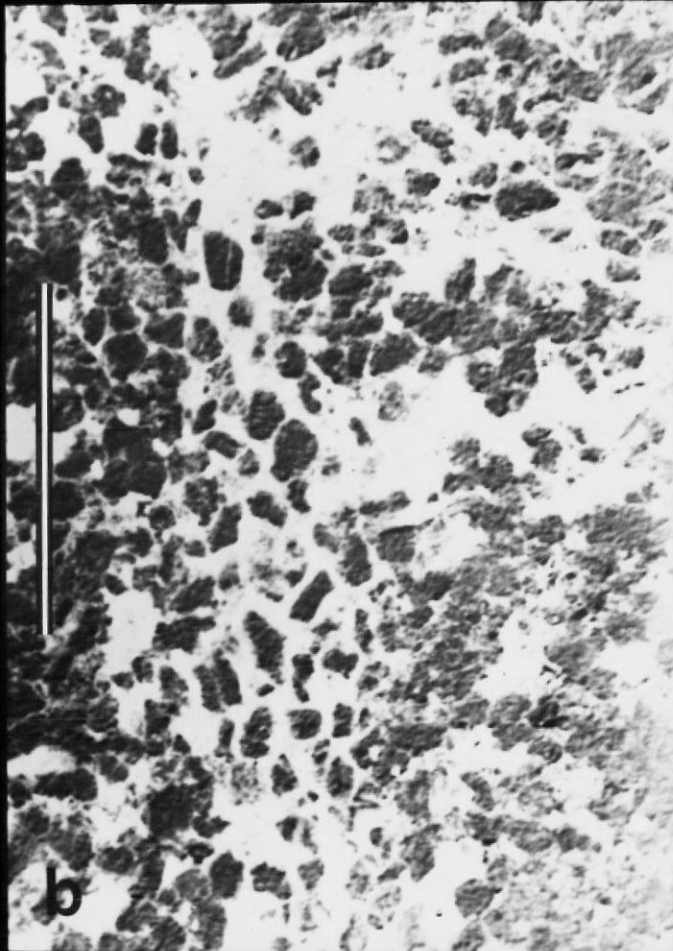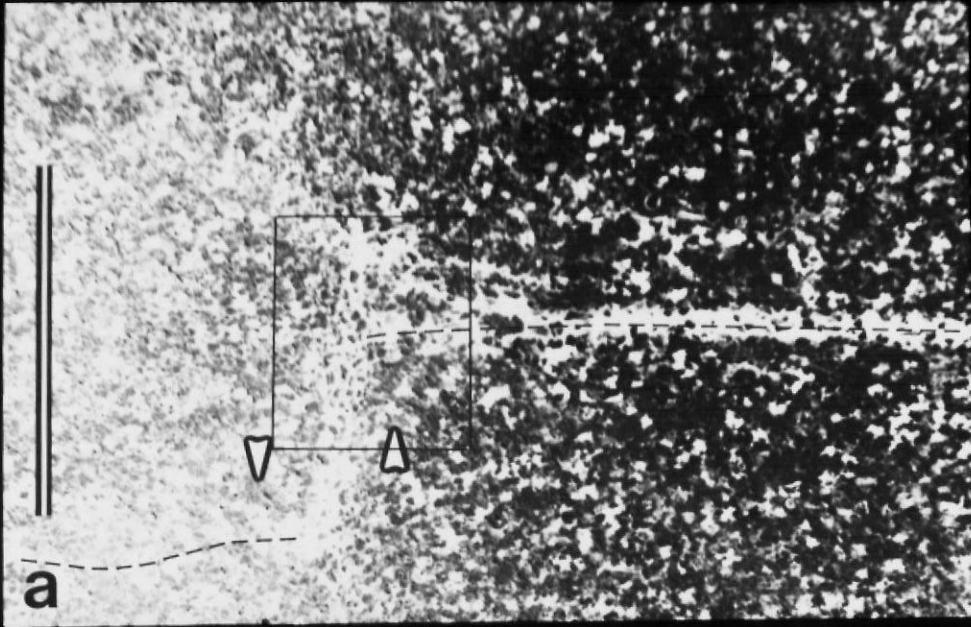
are generally not present in grains in the fault-zone, due perhaps to the abundance of clay or calcite coatings (the direct result of incorporation of those grains in the fault-zone).

These observations are significant substantiations of the field interpretation of the soft-sediment small-faults as soft-sediment feature. Observation (1) indicates that the sediment was cohesive enough to deform along narrow zones, a property which could be confused with tectonic deformation; (2) indicates the cohesion and frictional interlocking of grains was not great enough to favor grain fracturing and cataclasis over inter-granular rotations within the zone. From these observations, near surface deformation with attendant low confining pressure is implied. Observations (3) and (4) are significant in that they indicate the calcite and clay preserved the open packing of framework grains and that the faults occurred prior to quartz cementation. It is unlikely that the open packing could have survived much burial unless the infilling of clay and calcite occurred early in the burial history.

Claystone fabrics.

Deformed claystones collected from the basal decollement of the soft-sediment deformation localities at St. Johns and Ft. Defiance and those from a massive totally undeformed claystone near Nazlini, Arizona were compared. A major contrast is observed between the orientation of the clay platelets adjacent to the slickensided shear-surfaces and those immediately at shear-surface areas of the

deformed clay samples. The latter show extreme planar alignment, whereas platelets between the shear-surfaces show little to moderate alignment parallel to the shear-surfaces (Figure 20a). Totally undeformed claystones show no strong orientation of clay particles, only a slight sub-horizontal alignment, probably the result of compaction (Figure 20b).

Clay-platelet reorientation and shear motion between shear bounded "augen" are the operative deformation mechanisms when the claystones undergo shear-strain and flattening. It is important to note that these mechanisms of clay deformation have no implicit qualities which limit their occurrence to soft-sediment or hard-rock conditions. As a consequence they are not diagnostic criteria for the recognition of these features, found both in soft-sediment versus hard-rock deformities.

<div align="center">Hard-rock deformation.</div>

Features measured.

In order to compare samples completely, many deformation features were identified, counted, and measured. These features (1) calcite twin lamallae, in rocks containing calcite cement; (2) quartz deformation lamellae; (3) sets of near parallel microfractures in detrital grains, (some of the cracks are visibly open and filled with died epoxy, but most are closed and some are healed and marked by inclusions of impurities; (4) undulatory extinction in quartz grains; and (5) sharp or mosaic extinction boundaries within quartz grains. Features (1), (2) and (3) are used both as intensity-

Figure 20. Scanning electron micrographs of claystone fabrics from soft-sediment and undeformed localities. Shown are (a) oblique view of a corner of a clay fragment exhibiting slickensided shear surface (top of photo) with immediate transition into relatively undeformed inter-shear area (bottom of photo), (b) view of undeformed claystone shows random platelet orientations; viewing direction is parallel to strike, (c) also shown is a view normal to shear surface in (a) showing extreme alignment of clay-platelets on this surface, and (d) view normal to inter-shear surface in (a) showing very little clay-platelet reorientation. Scale bar in all photos is 10 microns.
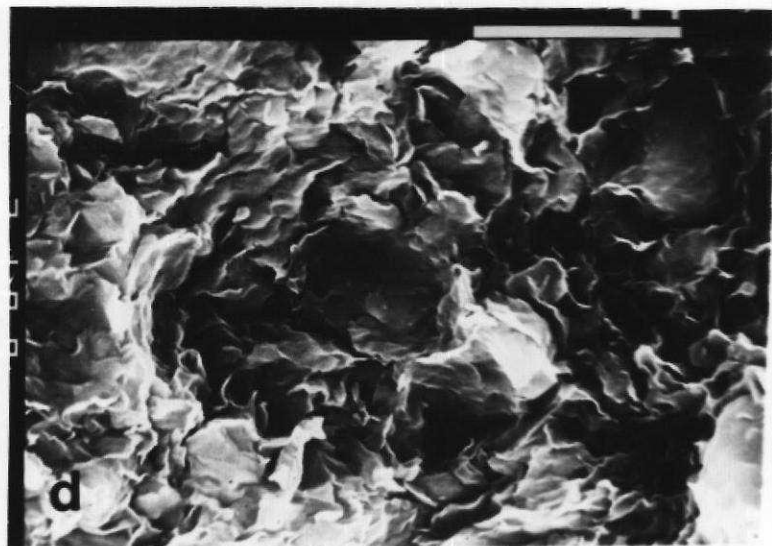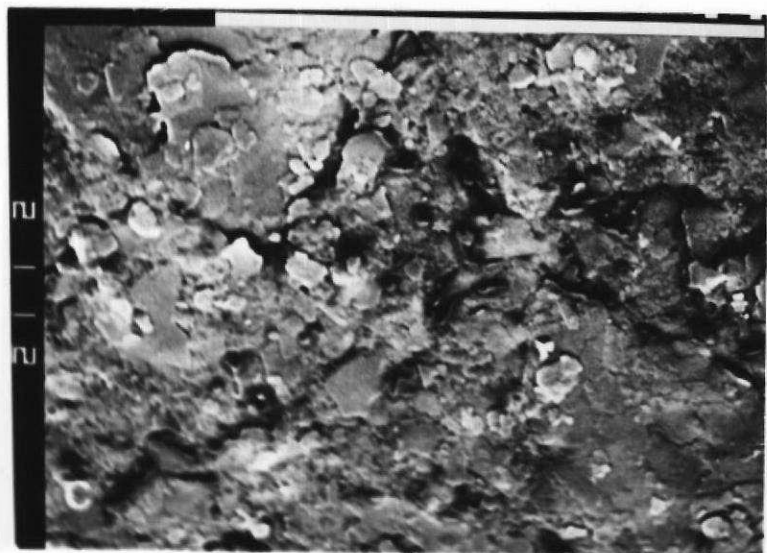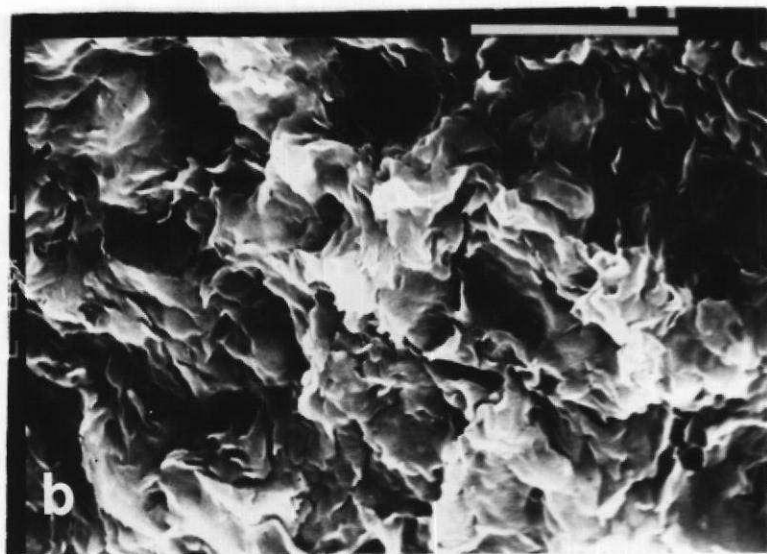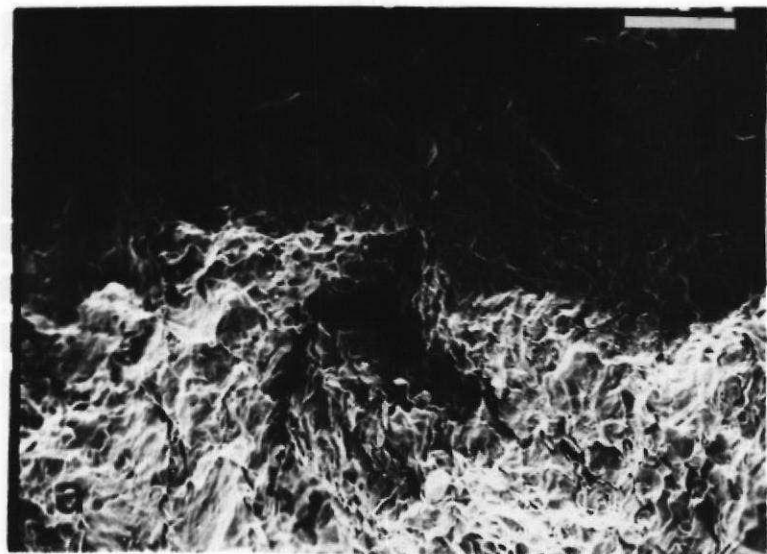
of-deformation and paleostress-direction indicators. Features (4)
and (5) are used only to evaluate relative intensity-of-deformation,
however the sharp extinction boundaries apparently also develop a
preferred orientation relative to the principal paleostress axes.
In addition to the five types of features described above it was
also useful to record the percentage of totally undeformed grains in
a given specimen.

Intensity of Deformation.

    Because no standard now exists for the relative comparison of
soft-sediment deformation to hard-rock deformation, it was necessary
to choose a reasonable initial standard of deformation intensity to
which all other deformation indicators could be compared. Since
hard-rock deformation is known to produce intragranular deformation
in grains that are previously undeformed, it is reasonable that the
abundance of undeformed quartz grains in a sample should be inversely
proportional to some function of the intensity of deformation. By
comparison to undeformed grain abundance the sensitivity and func-
tional relationship of the other measured features to deformation
intensity may be gauged. Qualitative field classification of local-
ities from which the samples were collected may also be directly
compared by this method.

    Obviously, an inverse correlation between the abundance of unde-
formed grains and grains with deformation features is expected with
increasing hard-rock deformation, i.e., deformed grains increase at
the expense of undeformed grains. The strength, however, of this

correlation is expected to be indicative of the sensitivity of each particular intragranular feature to the hard-rock.

Point counts were made of 150 to 300 quartz grains along linear traverses, in thin-sections from each sample. At least two orthogonal sections were combined for the counts from each sample. Polycrystalline quartz grains were excluded from the counts. Plots of the abundance of undeformed grains compared to the other five deformation features are shown in Figure 21. Important substantiation of the assumption that undeformed grains are indicators of hard-rock strain is given by the position of the samples from the three field classifications on these plots. Soft-sediment deformation samples (S_1, S_2, Figure 21) exhibit high percentages of undeformed grains, samples from over-printed localities (O_1, O_2, Figure 21) are in the intermediate range, and hard-rock samples (T_1, T_2, T_3, Figure 21, p. 95) contain intermediate to low percentages of undeformed grains. These trends are clearly evident even though some of the sampled features are no doubt relief from the source of the detritus.

In addition, these plots show that the most accurate and sensitive indicators of hard-rock deformation are the sharp or mosaic extinction boundaries, i.e., these data show the best inverse correlation (Figure 21a, p. 96). Jamison (1979) also noted a correlation between the abundance of sharp extinction boundaries and the relative degree of hard-rock deformation in a study of Laramide deformation of the Triassic Wingate Formation of the Uncompagre Plateau, Colorado. The second most sensitive indicator is the per-

Figure 21. Comparisons of the percentages of undeformed grains
to those with intragranular deformation features. Sharp extinction
boundaries in (a), microfractures in (b), undulatory extinction in
(c), and deformation lamellae in (d) are plotted against the per-
centages of undeformed grains. Range of percentages for a given
feature (ordinate) indicates relative sensitivity of each feature to
hard-rock strain. Symbols denote samples from the following local-
ities.

     Soft-sediment localities:

        S_1 = St. Johns

        S_2 = Many Farms

     Overprinted localities

        O_1 = Ft. Defiance

        O_2 = Navajo

     Hard-rock localities

        T_1 = Lupton

        T_2 = Ft. Defiance

        T_3 = 12 km north of Ft. Defiance

Each data point represents random counts of 150 to 300 grains
in at least two orthogonal thin sections.
* - Stars indicate samples with grains "floating" in matrix or
cement.

centage of fractured grains (Figure 21b, p. 91). The abundance of grains with quartz deformation lamellae (Figure 21d, p. 91) also shows a negative correlation although the scatter around the trend is large compared to the total range of percentages.

The relationships noted above are approximately linear (Figure 21a and b, p. 91). However, the relationship between undulatory quartz grains and undeformed ones appears to be more complex (Figure 21c, p. 91). With increasing hard-rock deformation (decreasing undeformed grain abundance) the abundance of undulatory grains reaches a maximum (35% undeformed grains), and then subsides to something below the level of the soft-sediment samples. The trend of sharp extinction features shows a flattening slope also around 35% undeformed grains. It is interesting to note that in the most deformed samples from hard-rock deformation localities, grains containing deformation induced crystal-plastic features (46%) are as abundant as those containing brittle deformation features (46% with microfractures).

Orientation of Features.

An important consideration in the use of the above features as indicators of hard-rock deformation is their orientational fabric. Deformation features which exhibit preferred orientation relative to the structural framework can be interpreted as having developed in situ as opposed to being developed elsewhere (relict) and trans- ported within randomly deposited detrital grains. Several of the samples which show well developed crystal-plastic features were

chosen for orientational analysis, of their orientation. Features whose orientations were measured are namely: (1) calcite twin lamellae; (2) microfractures; (3) quartz deformation lamellae, including both rotated and unrotated c-axis orientations (Carter and Friedman, 1965); and (3) sharp extinction boundaries, including c-axis orientations on both sides of the boundary.

Calcite Twin Lamellae. The orientations of twin lamellae in calcite grains have been used for some time to infer stress and strain axes (Turner, 1953; Groshong, 1972) in limestones. Twins also have been shown to be useful in determining stress-axis orientations in calcite cemented sandstones (Friedman, 1963). A plot of a large number of compression axes derived after Turner (1953) yields the general orientation of the true axis of maximum compression, provided that there is a large population of randomly oriented calcite grains in the previously undeformed rock. Extension axes are simply 90° to compression axes in the plane containing the normal to the twin plane and the c-axis.

The orientations of calcite twin lamellae were measured in the cement grains of a coarse-grained, calcite-cemented sandstone within the footwall, in close proximity to the east-dipping thrust fault at the Ft. Defiance hard-rock locality (Figure 12, pocket). The strike and dip of the bedding from which the sample was taken is N 28° W and 42° NE. Fifty-six percent of the calcite grains in the sample were found to be twinned; of these grains, 12 percent were found to have more than one twin-set. Plots of compression and extension

axes for this sample (Figure 22a and b) are widely scattered but indicate bedding parallel compression along an average axis oriented N 84° E (22° from the dip direction), and an average extension axis oriented normal to bedding. These data strongly indicate that the sand was cemented at the time of deformation.

Microfractures. The orientations of sets of microfractures were measured in samples containing abundant microfractures. A set is defined as two or more nearly-parallel fractures in a given detrital grain (Figure 23a). Some may extend into adjacent grains. Orientatations of normals to microfracture-planes (probably extension fractures) can used to infer the orientation of the least principal compressive stress axis in a grain and in the bulk sample when all grainfracture orientations are taken as a composite.

Microfracture sets were measured in the sample described above for which calcite twins also were measured. These microfractures are preferentially oriented parallel to bedding (Figure 24a) and indicate extension normal to bedding. These data are combined with those for microfractures in four other samples from the same locality in Figure 24b. These samples taken together also show microfractures subparallel to bedding.

Quartz Deformation Lamellae. Deformation lamellae have been used to identify principal stress axis orientations in naturally-deformed sandstones by Carter and Friedman (1965). Their C_1-C_2 technique involves determining the c-axis orientation of the host grain (C_1)
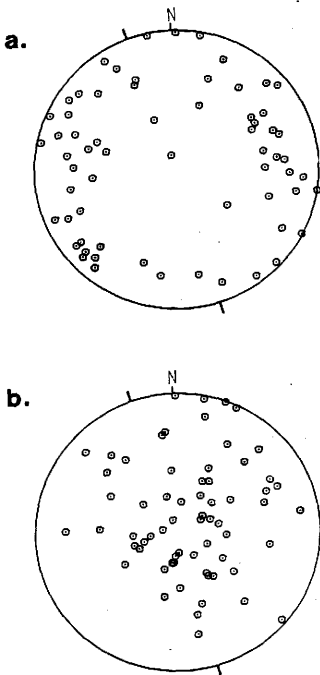
Figure 22. Equal-area lower hemisphere projection shows 66 calcite compression (a), and 66 extension (b) axes in calcite ce-mented sandstone from Ft. Defiance locality. Plane of projection is bedding. North is toward the top of the diagram; strike is indi-cated by the tick marks.

Figure 23. Photomicrographs of microscopic hard-rock deforma-
tion features in quartz grains in samples from the Ft. Defiance lo-
cality show (a) microfracture sets in quartz grains (scale bar is
.25 mm), (b) sharp extinction boundary in quartz grain (scale bar is
.25 mm), (c) example of quartz grain with a noticeable translation
along sharp extinction boundary (translated portion actually induces
a similar response in an adjacent grain [arrow], scale bar is
.25 mm), (d) hard-rock small-fault demonstrating (i) grainsize re-
duction across boundaries (straight arrows) and (ii) grain disinte-
gration by both brittle and crystal plastic mechanisms (curved ar-
rows) (scale bar is .5 mm), (e) quartz grain demonstrating both
cracking (straight arrow) and tilt boundary formation (curved arrow)
(scale bar is .25 mm), and (f) small hard-rock fracture demonstrat-
ing, grain-boundary and transgranular cracking and fracture-parallel
microfractures (scale bar is .5 mm).

a

b

c

d scale

e

f
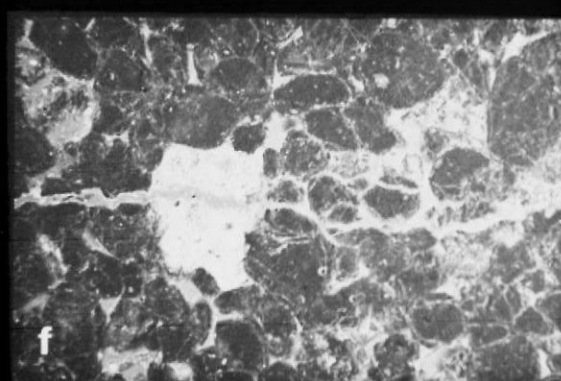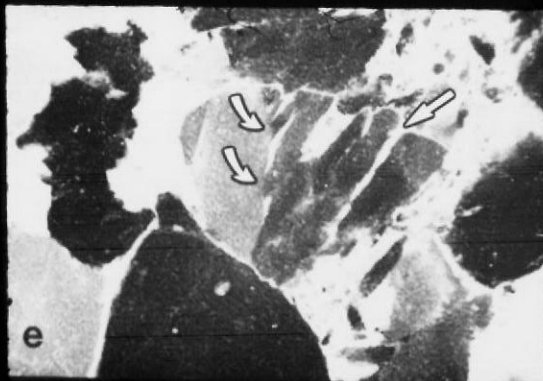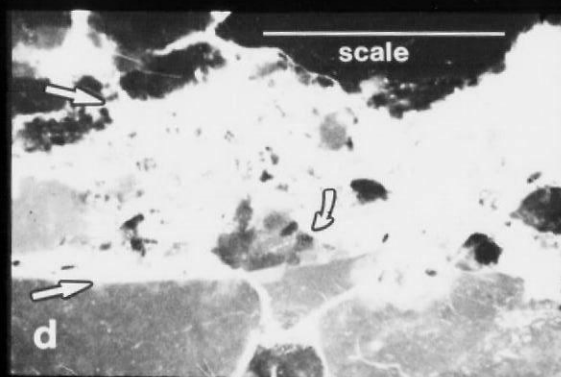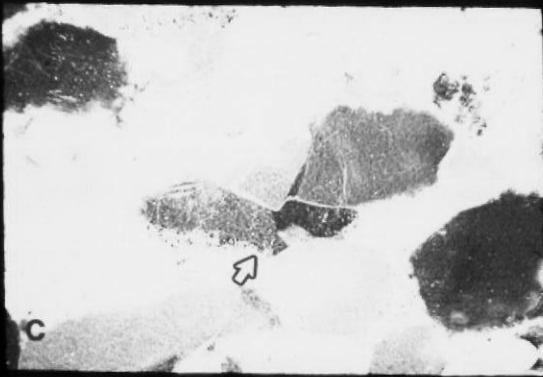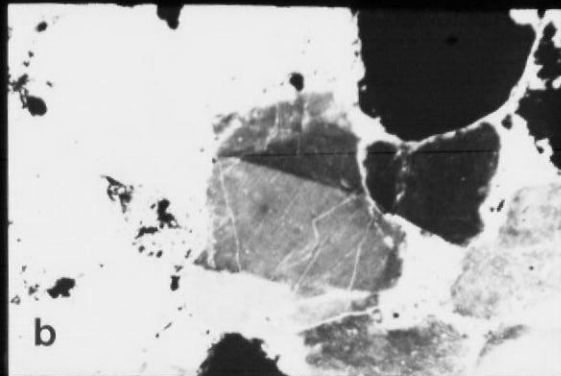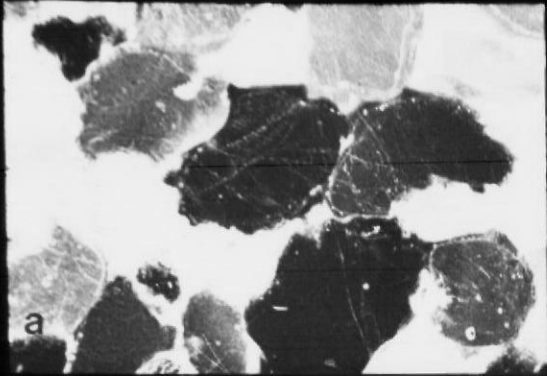
Figure 24. Equal-area lower hemisphere projection of orienta-
tions of various hard-rock quartz deformation features. Plane of
projection is the bedding-plane; north is towards the top of the
diagrams. (a) 75 microfractures from sample whose calcite fabric is
shown in Figure 23, p. 102; strike is shown by tick marks; (b) com-
posite diagram of 398 microfractures from 5 samples (including that
in (a) from the Ft. Defiance hard-rock locality; (c) C_1 (small
circles) and C_2 (large circles) c-axis orientations from grains
with deformation lamellae are connected by great circles; the C_2
end of each data pair tends to point to the greatest principal com-
pressive stress (within dotted circle, after Carter and Friedman,
1965); (d) 103 microfracture poles from same sample observed in (c);
rough N-S girdle of poles also indicates a maximum principal com-
pressive stress with a similar orientation to that in (c) (dotted
circle)
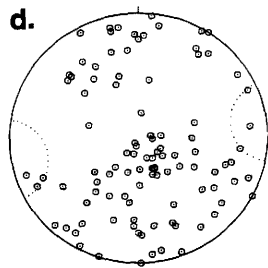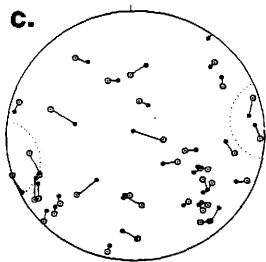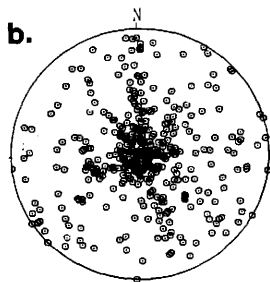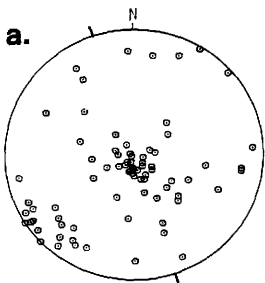
and that of the rotated portion (area of closely-spaced deformation lamellae) and graphically connecting these c-axes on a stereonet along a great-circle. They demonstrated that the rotated end of the great-circle (C_2) points to the orientation of the maximum principal compressive stress. The rationale behind this procedure is as follows: The zone containing the deformation lamellae is essentially a "kink-band" where the slip surface is the [0001] basal plane (subparallel to the lamellae) of the quartz. The normal to the slip surface in the kink-band (C_2) rotates toward the maximum principal compressive stress axis. Thus all great-circle traces connecting the C_1 and C_2 axes should point toward the orientation of the maximum principal compressive stress. This technique was used in the analysis of a sample taken from a sandstone striking N 52° W and dipping 75° E in the Lupton hard-rock deformation locality. (Figure 24c). This plot shows that C_1-C_2 great-circle directions tend to point out a compression direction bearing approximately N 101° E and nearly parallel to the bedding plane. Comparison of this pattern with the wide north-south girdle of microfracture poles in the same sample (Figure 24d, p. 99) which indicate a principal compression axis bearing approximately N 80° E and layer-parallel, substantiates a roughly east-west layer-parallel, maximum principal compressive stress direction for this sample. Macroscopically this E-W compression is nearly perpendicular to the local fold (monocline) axis.

Sharp Extinction Boundaries. The abundance of sharp or mosaic ex-
tinction boundaries in quartz grains and their apparent sensitivity
to the magnitude of hard-rock strain (Figure 21a, p. 91), warrants
further characterization of their orientational development. Sharp
extinction boundaries are subplanar low angle tilt boundaries in a
grain across which there is a small angle of crystallographic
disorientation (Figure 23b, p. 97). The orientations of these
boundaries have not been measured in rocks to the best of my know-
ledge. Accordingly, these boundaries were measured in the most
severely deformed sample hard-rock deformation sample from the Ft.
Defiance locality in order to determine their possible dynamic sig-
nificance.

   Comparison of the angles between the c-axis and the poles to
the extinction boundaries in individual grains reveals that many,
but not all, of the boundaries are prismatic (Figure 25a). In order
to relate the rotations of the c-axis across these boundaries, the
angles between the rotation axis and the pole to the boundary-plane
were plotted (Figure 25b). The former is the pole to the great-
circle through the c-axes on either side of each boundary. This
relationship permits recognition of the crystallographic slip
systems which operated to achieve the rotation. If slip on [0001]
was the only slip system active in these grains during formation of
the sharp extinction boundaries, the axis of rotation of the c-axes
across each boundary should lie in the plane of the sharp extinction
boundary, i.e., 90° to the pole of the extinction boundary. This is
the case for most of the rotation axes (Figure 25b), however a sig-

a.

ANGLE BETWEEN C-AXES AND SHARP EXT. BOUNDARIES

b.

ANGLE BETWEEN ROTATION AXES AND SHARP EXT. BOUNDARIES
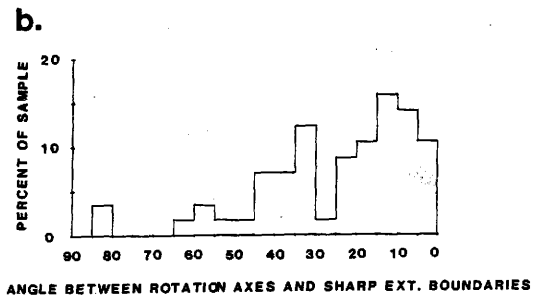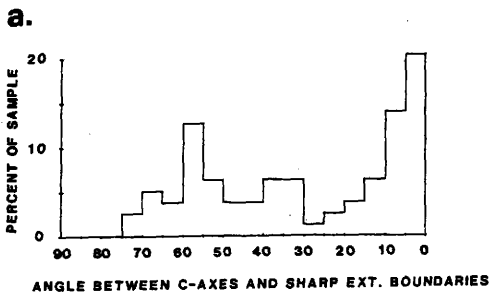
Figure 25. Histograms of the angle between the c-axis and sharp extinction boundary for (a) 150 measurements (b) 88 measurements.

nificant number of rotation axes are not near 90° to the boundary-plane pole. Additional non-basal slip systems must have acted in order to allow rotation axes to lie at angles to the boundary-plane, including possible rotation on the boundary itself. Christie and others (1964) have experimental evidence for minor slip on addition-al systems in quartz under conditions where basal slip is dominant. Some grains in the above sample also show considerable intragranular translation on the extinction boundary plane (Figure 23c, p. 97). That these translations are not associated with any visible crack-ing, suggests they may be due to crystal-plastic behavior. Small rotations associated with this translation could account for some grains which demonstrate rotation-axes that are not in the boundary-plane.

The c-axis of the host grain (as opposed to that of the rotated portion of each grain) could not be identified across the sharp ex-tinction boundaries. If it had been possible to identify a host c-axis then Figure 26a could have been used as a C_1-C_2 diagram for quartz deformation lamelae of Carter and Friedman (1965) (Figure 24c, p. 99). Without a host designation the great-circles (Figure 26a) point either toward the maximum or the minimum principal com-pressive stress depending upon which side of the boundary rotated with respect to the external coordinates. The great-circle traces in Figure 26a show a general N 75° W - S 75° E trend with a center of gravity that plunges about 15° to the N 75 - 80° W. Layer paral-lel microfractures from this sample and those in this area (Figure 24b, p. 99) confirm nearly layer-parallel compression subparallel
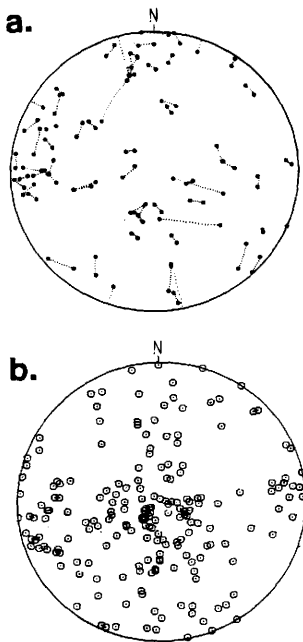
Figure 26. Equal-area lower hemisphere projections of c-axis orientations and poles to sharp extinction boundaries show (a) 60 pairs of c-axes across extinction boundaries connected by great circles for a sample from the Ft. Defiance hard-rock deformation locality, and (b) 204 poles to sharp extinction boundaries in the same sample as in (a).

to this same bearing. The orientations of extinction boundaries from the same sample show prominent (but diffuse) patterns that include a set normal to the inferred maximum principal stress and a set subparallel to bedding (Figure 26b). These patterns are similar to those of the c-axes of the grains which contain the extinction boundaries (Figure 26a). Thus, the orientational fabric of sharp extinction boundaries appears to not only demonstrate ordered development but may possibly have dynamic significance.

Further observation of sharp extinction boundaries and detailed substantiation of the crystalline mechanisms involved in their development are beyond the goals of this study. The significant conclusion of the above observations is that identification of the ordered development of importance here is the fact that these extinction boundaries exhibit a preferred orientation. Accordingly they were formed in situ (rather than being relict) and clearly are the result of hard-rock deformation.

Hard-rock Small-faults.

Hard-rock small-faults, small gouge-filled faults in sandstones, have been recognized earlier as indicators of hard-rock deformation and have been investigated by Aydin (1977) and Jamison (1979), who discussed the microscopic properties of the hard-rock small-faults in Mesozoic sandstones of the Colorado Plateau deformed in the Laramide. Their microscopic observations are consistent with those of samples in this study as summarized below:

(1) well defined boundaries delineating a fault-zone less than
    1 mm wide are present in most hard-rock small-faults;

(2) evidence for grain disintegration, comminution, rotation
    and recementation of the grains (primarily quartz) within
    the fault is present in all cases; and

(3) both brittle and crystal-plastic mechanisms, particularly
    sharp extinction boundary formation, are abundant in quartz
    grains within 2 mm of the fault as well as within the band
    itself.

The most striking microscopic feature of the hard-rock small-
fault is the dramatic grain size reduction across it's boundary with
the host-rock (Figure 23d, p. 102). Observation of individual
grains indicates that this is accomplished by both brittle cracking
and the formation of and translation on sharp extinction boundaries
(Figure 23d and e, p. 102). Because hard-rock small-faults occur
only in the most highly deformed rocks, their use as a hard-rock in-
dicator is limited to high-strain areas. Nevertheless, their ident-
ification in both outcrop and thin section is unmistakable, due to
the contrast in the properties of the host rock and fault-zone
materials.

Fractures.

Open macrofractures were designated in the field as features
that developed during deformation of "hard-rocks." Thin sections
across these fractures show the following: (Figure 23f, p. 102).

(1) an open fissure (filled with died epoxy) is bounded by the fracture surfaces;

(2) the fracture itself consists of both grain-boundary and intragranular segments, resulting in a fairly linear trace even on the microscopic scale; and

(3) microfractures in grains in the near vicinity of the fracture surfaces are parallel to the fracture trace.

The characteristics outlined above indicate the rock was cemented, at the time of fracture.

Summary.

In summary, (1) microfractures, (2) sharp extinction boundaries, (3) deformation lamellae, (4) undulatory extinction, and (5) calcite twin lamellae can all be used confidently to identify "hard-rock" deformation of sandstones microscopically. This can be done on the basis of both abundance, as well as orientation of these features. In samples where dynamic interpretation of orientational fabric was made, roughly east-west, layer-parallel compression is found, regardless of the geographic location of the sample along the East Defiance Monocline.

Hard-rock small-faults and open fractures, both designated as hardrock features in the field are shown here, microscopically, to be the result of deformation of an indurated sandstone, probably at elevated confining pressure. As a result, both of these features are confirmed as indicators of hard-rock deformation, as suggested

by their field occurence. Soft-sediment small-faults are revealed,
by their microscopic appearance, to be the result of deformation of
a cohesive but uncemented "soft-sediment" at low confining pressure
(also suggested by their field occurence) and are confirmed as a
diagnostic soft-sediment deformation indicator. Slickensided shear-
surfaces in claystones appear to be qualitatively indistinguishable
down to the sub-microscopic scale, regardless of the environment of
deformation. Thus, it is best to use deformation features in sand-
stones in order to evaluate the type of deformation present in a
given area, relying on microscopic observation for substantiation of
macroscopic, field classifications.

CHAPTER IV

MODEL STUDIES AND FIELD COMPARISONS

Introduction.

    A series of physical models were constructed and studied with a
view toward augmenting the field and microscopic studies to gain a
more complete understanding of the mechanical response and loading
conditions which led to the development of features observed in the
field. Because deformational features on several scales are inter-
related in their natural occurrence, features on a variety of scales
are also addressed in the models. The models presented here by no
means address all of the features, both hard-rock and soft-sediment,
observed in the field; they do, however, clarify some concepts
pertaining to important aspects of the kinematic development of both
hard-rock and soft-sediment features.

    The advantages of physical models are that they allow the unan-
ticipated as well as the anticipated responses of the components to
be manifest. In physical modeling, because of the relative inability
of the experimentor to control the interactions of the components
once the experiment (model) has begun, naivities are revealed and
insights are reinforced by the final outcome. Although countless
initial biases and assumptions go into the construction of a model,
the operational phase is of much use in educating the experimentor.

The number of features that can be confidently addressed with a physical model depends on the complexity of both the natural feature being modeled and the model, and to a certain extent on the confidence which the experimentor places in his modeling technique.

The models presented below are composed of a variety of materials ranging from potter's clay to rock-materials and lead. The materials are chosen on the basis of their response to deformative stress (i.e., relative-strengths, flow versus faulting) and are not meant to be truely scaled models.

The models range in size from 2 x 5 x 15 cm for the rock-material models to 4 x 35 x 40 cm for the clay models. The clay models are deformed at or near atmospheric pressure whereas the rock-material models (isolated from a confining medium by polyolefin jacketing) are deformed at 80 MPa confining pressure. Specific components and conditions are described for each model in the sections to follow. The primary variables in these physical structural models are:

    (1) The absolute and relative material-properties of the components, i.e., relative strengths and ductilities.

    (2) The geometry and magnitude of the externally applied loads.

These variables are intentionally constrained by initial model-design but are allowed to freely interact during the kinematic operation of the model.

Soft-Sediment Models.

Plate-bending Model.

From the field and laboratory observations it was determined that soft-sediment small-faults are the most diagnostic feature of the soft-sediment deformation in sandstones. Because of the consistent symmetry of the small-faults with respect to the strike and dip of bedding it is possible these faults accomodate strains required by the bending of the beds. This "bending-plate" interpretation is especially apparent in the Agathla Peak area where a single bed shows category 2 normal-faults at the top and low angle normal-faults at the base. The most reasonable interpretation of this phenomenon is that the fault orientations in lower beds were modified by inter-layer slip due to bending of the unit. It has been shown that there was probably a very low effective confining pressure under which the deformation took place. Also, it is apparent that the sandstones were cohesive enough to fault rather than flow (by intergranular rotations and translations), but due to lack of cementation and pressure did not deform as hard-rocks.

Accordingly, a model was designed to test the following: can soft-sediment small faults be produced purely by bending in a cohesive (but not cemented) plate of material under very low confining pressure? This seems to be the most reasonable interpretation or conceptual model based on field observation.

The material used for this model was potter's clay which was mixed in a ratio of 5:1 by volume (powdered clay to water). The

mixed clay was spread into a cake approximately 3.25 cm thick by 35.5 cm in width and 28 cm in length. Two cakes of this dimension were constructed. One was a solid clay cake, the other was separated into two layers of equal thickness by a sheet of acetate. The clay was chosen because it is easy to work with and has low strength and cohesion. (The potter's clay does fault quite readily in extension at a critical extensive strain of approximately 5%.) Thus, this material meets the requirements desired of the material component. It should be noted that the analogy of the clay in the model to the sands in the field is one of cohesive material-response not texture or composition. Both the clay in the model and the sands in the field are observed to deform discontinuously by faulting.

The loading condition for this model consists of passive-bending of the clay cake in order to evaluate the validity of the assumption that the faults are the direct result of only bending-stresses and strains produced at or near the surface. In order to produce this loading, an apparatus was built that bends a plate of sheet metal into an anticlinal form at a constant bending-rate while maintaining a smoothly rounded surface (Figure 27c). The apparatus is designed so as to bring two points on the steel bed (limbs of the anticline) toward each other at a constant rate by a motor-driven screw-drive. The clay cake rides passively on this plate and bends as a consequence of its own weight by keeping its lower surface in contact with the surface of the sheet metal, i.e., the clay-cake is not "end-loaded". Bending stresses only (except for shear stress

due to flexural slip on the clay-metal boundary) and low pressure

(atmospheric) deformation are achieved with the above model assembly.

The model bend (fold) varied from an initial interlimb distance

of approximately 54 cm to a final distance of 23 cm. At higher

curvature the clay begins to pull away from the metal plate. At the

initial stages of bending the clay shows no fault features, accord-

ingly the following discussion will be restricted to the

intermediate to final stages of bending.

Results.

The features developed on the upper surface of the cakes are

small normal-faults (Figure 27a). These faults are slightly

undulatory in strike but parallel to the fold axis. They all show

normal dipslip displacement and have striated scarps which confirm

the slip. In cross-section the fault displacements die out toward

the lower surface of the clay cake. Individual fault scarps may be

as long as 15 cm and have as much as 5 mm vertical throw before the

fault surfaces begin to separate, leaving an open fissure. The

strikes of some faults tend to curve toward the down-thrown block

near their terminations. It is concluded that these soft-sediment

small-faults are due to extension of the upper fiber of the fold due

solely to bending. Both the single-layer and two-layered clay cake

models produced the same style of soft-sediment small faults on the

upper surface, however those in the two-layered model occur at a

slightly higher bed-curvature than those in the single cake and do

not achieve as great a final throw on individual faults as the

Figure 27. Deformation features in clay models and apparatus
used to deform them. (a) Top view of clay cake subjected to anti-
clinal bending produced small normal fault sets (parallel streaks
are the result of the final trowel stroke in shaping the clay cake);
(b) side view of two-layered model shows modification of fault
traces due to slip between layers; (c) photo shows apparatus used to
deform clay models; (d) side view of clay-sand-clay layered shear-
zone displays fault geometries; (e) partial and (f) complete section
through shear-zone model shows nature of deformation of sand layer
due to listric faulting; scale bar in (a), (b), (d), (e) and (f) is
5 cm.
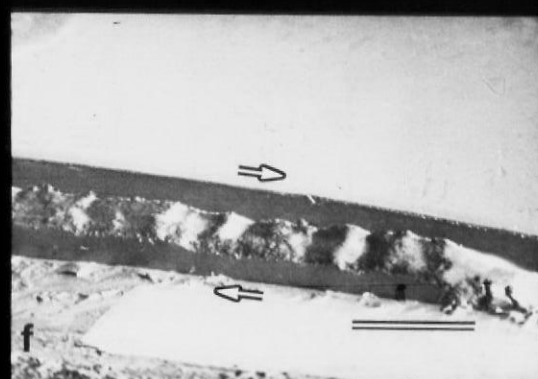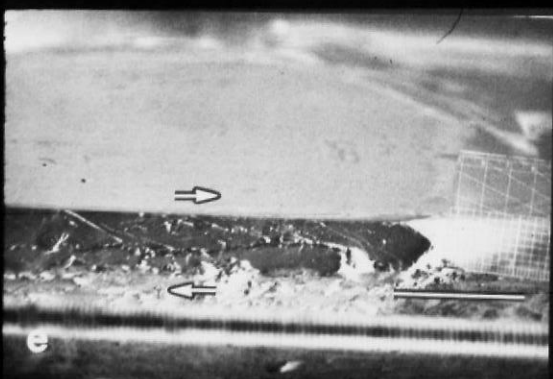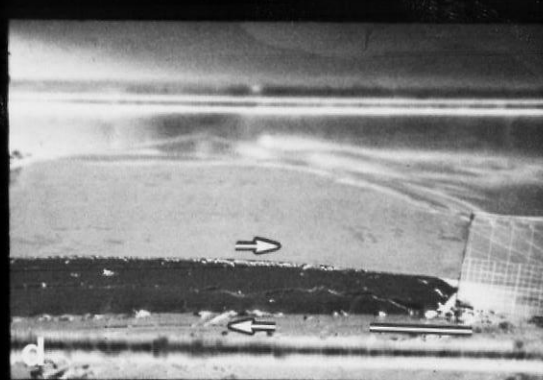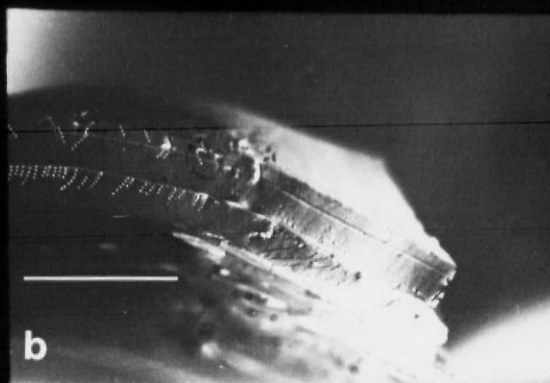
single cake model. The faults serve to extend the upper surface of the fold normal to the axis in both the single and double layer models.

In the double-layer model soft-sediment small-faults in the lower layer are modified by flexural slip on its upper and lower contacts during folding. The soft-sediment small-faults in the lower layer are dominated by a single conjugate of the normal-fault set. These normal faults are disposed at a lower angle to the layer with increasing distance from the axis of the fold and always dip away from the direction of layer dip. The magnitude of interlayer slip appears to be the primary factor influencing the orientation of faults in the lower layer. The faults in the upper layer are identical to those developed in the single-layer clay cake and consist of well-developed conjugate pairs that maintain constant orientation relative to the layering and constant density where the layer's curvature is constant. The density and orientation of these faults in cross-section can be seen in Figure 27b p. 115.

Comparison with Field.

The soft-sediment small-fault development in the model is very similar to that found in the field where soft-sediment small-faults are the main criteria for soft-sediment deformation. Faults in both the field and the model show dip-slip displacements that extend the bed perpendicular to the fold axis. In addition, faults in the model show strikes, morphologies, and geometries that are nearly

identical to the category 1 faults found in the upper decollement surface at the Ft. Defiance soft-sediment locality (Figure 10, p. 45).

The faults observed in cross-section in the two-layer model are quite similar to those observed in the two-layered unit which out-crops in the Agathla Peak area (Figure 10c, d, p. 45). This model points to the fact that the low-angle conjugate developed in the massive sandstone at Agathla Peak (similar to faults at St. John's) may be the direct result of flexural-slip between layers during folding.

The smooth curvature of the model is unlike the sharp hinges and chevron folds observed in the field. Nevertheless, similar more restricted regions of bending-stress are present in chevron folds. These isolated regions are the sites where the soft-sediment small-fault intensity is high in the field.

Unlike the natural situation, the model did not produce fault geometries like those of category 2 or 3. The reason for this lack of geometrical correspondence between the model and natural faults is open to speculation. Dip-slip on category 2 or 3 faults produces shortenings or elongations parallel to the fold axis. Because the model apparatus was unable to impose similar strains on the clay cakes it is not known whether category 2 or 3 fault geometries could develop in a model with axis parallel strains. Oertel (1965) interpreted an orthorhombic pattern of faults in his extended clay cakes due to fault interference. The faults in the upper surface of the clay cakes in this study are similar to those of Oertel from

which he interpreted a family of four fault orientations. The undulation in the fault surfaces in my models is not believed to be significant enough to separate into four individual fault orientations. This conclusion is based upon the field observation that single fault-planes in any one position of the category 1 through 3 arrays in the field show as much strike undulation as those in these models and those of Oertel (1965) (Figure 11d, p. 50).

The geometries of the soft-sediment small fault arrays may be significant in their implications toward the development of natural fault systems. Bishop (1953) showed that any constant volume, three dimensional deformation requires at least 3 slip planes determined by 5 independent slip systems. In addition, Reches (1978) showed that, if the deforming body was constrained with respect to boundary rotations then 4 fault-planes with orthorhombic symmetry are required. If the strain is two dimensional, these solutions reduce to two dihedral-planes, both normal to the plane of strain (Coulomb conjugate-shear geometry), such as those produced in the above model. The soft-sediment fault geometries observed in the field are those predicted by Reches (1978), and suggest application of the theories of faulting involving a three dimensional strain-field to naturally deformed materials is valid. However, outcrops which show more than four fault-plane orientations are not explained by these theories or the models, if all faults developed simultaneously.

General correspondence of soft-sediment small-fault morphology, density, position and orientation between the models and field is

very good. Such close correlations warrant the interpretation that
the observed natural soft-sediment small-faults could be the result
of bending-stresses on cohesive but uncemented materials at low
confining pressure. The model results also are consistent with the
view that flexural slip may be responsible for the low angle faults
that occur in lower beds of massive sand units.

Layered shear model.

At both St. Johns and Ft. Defiance, decollement surfaces bound
the top and bottom of a deformed zone that must have developed
before the sediments were lithified. Several lines of evidence such
as (1) the small subsidiary chevron-folds in vertical sand beds at
St. Johns; (2) clay shear-textures at St. Johns; and (3) simultaneous
development of soft-sediment small-faults along with the upper de-
collement surface at Ft. Defiance, suggest that the middle structural
unit deformed at least partially in response to opposed senses of
shear at the upper and lower decollements. Moreover, the strain
plan most descriptive of the deformation involves shear. One
difficulty in constructing a corresponding physical model lies in
determining a reasonable initial geometry of material components.
Reconstruction of pre-shearing geometry from a highly deformed field
setting is difficult because the amount of pre-shear deformation is
unknown. As a result the initial geometry used in the model was
that of flat-lying layers of contrasting materials. This approach

permitted me to examine the hypothesis that absolutely all of the deformation occurred in a shallowly-buried shear zone.

The materials used to represent the layered section consist of a layer of fine-grained moist quartz sand approximately 3 mm thick imbedded between two layers of potters' clay approximately 2 cm thick. The total cake width and length are 30 cm and 35 cm respectively. The relative mechanical properties of the sand (slightly stronger and less ductile than the clay) and clay in the model are considered similar to those of the sands and clay in the field. The sand in the model was moistened in order to make it slightly more cohesive than dry sand. A material property not included in the model was that of fine layering. Because the effects of multilayer folding would have required a much more complex component-package, it was determined that a thin layer (3 mm) of sand would allow greater scale of observation and permit a great magnitude of shear-strain to be imposed. If a thin layer would fold, it was reasoned that a layered unit will probably do the same, provided they are both isolated from the shear surfaces by the same material (clay).

The apparatus used to apply the load (Figure 27c p. 115) is the same as that used for the plate-bending model. It is modified by attaching a stationary metal plate to the stationery frame. A separate metal plate is attached to a screw driven cross-rod. The driven plate can be drawn at a constant rate parallel to and above the lower plate. By placing the layered clay/sand package between the two plates and adding weights (75 lbs. of flat rock slabs, larger than the clay cake), and displacing the upper plate, cons-

tant-rate, shear-loading can be imposed on the package. The upper plate was displaced 25 cm with respect to the lower plate at a rate of approximately 2.5 cm/ minute. Due to some slip of the upper and lower plates at their contact with the clay, exact shear strain within the unit could not be accurately determined, but opposite senses of shear were obtained at the top and bottom sand/clay interfaces.

Results.

Under these conditions the sand/clay model elongated approximately 17%, primarily by sliding of the upper clay layer over the lower by detachment at the base of the sand. No buckle-like bending occurred in the sand, however the sand did take on a macroscopically underlatory appearance (Figure 27d, p. 115). This appearance is the result of evenly spaced listric normal-faults in the upper clay layer that cut through and flatten into the base of the sand layer (Figure 27e, p. 115). The undulations in the sand layer are caused by rotation of inter-fault domains of sand along the fault-surfaces. The concave-upward faults originate at the upper shear surface and dip only in the direction of movement of the upper plate. The topographic character of the sand layer is shown in Figure 27f (p. 115.). Additional faults originate at the base of the sand and cut the lower-clay layer to the lower plate surface. These dip in the same direction as those above but generally are not curved in cross-section. All of the faults serve to extend the package. Folding (shortening) is not observed in this model.

Comparision to the Field.

This model presents essentially no comparable features to those observed in the field. The only extensional features observed in the field are the small faults which have been linked to local bending (over all shortening). Because the model shows only low-angle normal-faults (Riedel, R_1 faults), it is determined that the loading conditions used in the model are an invalid explanation for the features observed in the field. Field evidence does suggest that shear conditions did exist at sometime during the soft-sediment deformation. Possible explanations for the differences between the model and the field structures are:

(1) In the model, there is no lateral constraint of the layers in the direction of shear (simple-shear). If there was such a constraint in the natural system (i.e., a pure-shear component) perhaps there would be a thickening of the zone (observed at St. Johns) resulting in the production of folds.

(2) At St. Johns and in the Navajo Roadcut there are angular unconformities at or near the top of the folded middle structural unit. This fact suggests that at least some (perhaps most) of the soft-sediment folding occurred prior to deposition (or emplacement) of the upper structural unit. Further decollement sliding could have slightly modified the initial deformation and produced the evidence of shear on both upper and lower decollement surfaces. This interpretation permits the lower

decollement to result from initial gravitational sliding
and to be followed by erosion, deposition and subsequent
movement on the upper decollement.

The second explanation is preferred here because of the circum-
stantial evidence of angular unconformities in the localities in-
vestigated. Nonetheless, similarity of upper and lower decollements
leaves open the possibility of considerable modification of the fea-
tures by post-burial sliding on both surfaces.

It is not possible to make an assessment of the relative con-
tribution of pre-burial, slope processes (slump folding) and early
post-burial processes (shearing) from the above model study. It is
possible to say that both processes may have contributed to the soft-
sediment deformation in both the Ft. Defiance and St. Johns areas,
and possibly the other soft-sediment localities.

Hard-rock Deformation Models

Description.

The hard-rock structures in the Chinle Formation described
earlier were located on the east-dipping flank of the East Defiance
Monocline. The macroscopic style and scale of the structural
features in the Ft. Defiance area are such that they could be
confused with structures in soft-sediment localities. The hard-rock
deformation in the area northeast of Ft. Defiance is linked to
Laramide faulting and imbrication within the Chinle Formation, pri-
marily the lower part. Here and to the south (Lupton area) extreme

thickness variations have been measured within the Chinle. These variations suggest that flow and detachment necessary for the kinematic development of the East Defiance monocline may have been localized within the Chinle Formation, resulting in complex tectonically-induced folds, faults and truncations. By comparing the structures of the East Defiance Monocline, with those due to localized detachment within an appropriate model one can qualitatively evaluate the importance of detachment and thickness changes toward the development of the Monocline.

Kelley (1967) suggested that the sinuous nature of the East Defiance Monocline was due to right-lateral strike-slip motion along a frontal NNE trending boundary fault. Kelley reasoned that wrench faulting at depth along the trace of the monocline would produce folds which trend obliquely across the hinge of the monocline and die out along their strike away from the monocline. For folds of this type to develop the folded zone must be detached from the underlying wrench-faulted basement blocks. With no detachment only a suite of faults characteristic of wrench-fault areas would develop. (Wilcox and others, 1973).

Design of a model to test the effect of wrench-motion on features in rocks isolated from the wrench fault by a detachment horizon, was the major objective of this portion of the model study. In the resulting model design, displacement is induced along a precut "wrench-fault" in forcing blocks and the layers overlying the fault are allowed to deform in response to the wrench or oblique-slip motion.

Following the basic design of Bartlett and others (1981); three model configurations were used, (exact configurations and dimensions are shown in appendix A.). The basic components of this model consist of a precut sandstone block, 12.7 cm to 15.3 cm long and 9.0 mm thick which is overlain by a lead veneer 1.1 mm to 2.2 mm thick. The lead (detachment horizon) is overlain by either a limestone unit (2.5 mm thick) or a mica layer. (.8 to 2.9 mm thick). For the latter both biotite and muscovite were used. All these models were deformed in the high pressure apparatus described by Handin and others (1972) at a constant displacement-rate of approximately 10^{-3} cm/sec and a confining pressure of 70 to 80 MPa. The models were isolated from the surrounding pressurized confining fluid by a relatively strengthless polyolefin jacket. The confining pressure provided high enough normal stresses between the components to impede separation or slip at their boundaries and it has no relation to the overburden pressure under which the laramide features deformed.

Results.

The first model (model I) consists of a forcing block assembly identical to that used by Bartlett and Friedman (1982) (Appendix). The top and bottom of the forcing blocks are covered with lead beneath either limestone or biotite, one on the top, the other on the bottom of the model. The sample was constructed such that the biotite and the limestone were the same length as the forcing

block. This configuration places an end-load on the layers and constrains their rotation during deformation.

Two kink-folds are produced in the lead-biotite veneer at 45° to the underlying fault (Figure 28a). These folds die out away from the fault. On the opposite side of the model, a 2 mm wide wrench-fault zone developed in the lead-limestone veneer, immediately above the trace of the fault in the forcing block (Figure 28b). The difference in response of the two veneers is attributed to the ability of the biotite to fold by flexural slip along it's basal cleavage. Since the limestone does not have this potential it faults, despite comparable isolation from the forcing-blocks by the detachment horizon (the lead). This experiment serves to point out the necessity of both a layered unit and a detachment horizon in order to produce folds over a strike-slip fault.

The axes of the kink folds in this first model are normal to the loading axis of the model-assembly, and thus could be interpreted as the result of end-loading only. In order to test the effect of the strike-slip faulting without direct end-loading, a slightly different configuration (Model II) was designed in which the mica veneer is not end-loaded and is allowed to rotate about an axis perpendicular to the mica sheet (Appendix A). As a result the mica sheet is loaded only by shear-stress transmitted through the lead layer. The resulting structures are similar to those of the first model with two major exceptions. (1) Deformation due to wrenching is confined to folding and faulting at one end of the specimen and to simple layer parallel rotation at the other end due to lack of

Figure 28. Photographs show structures developed in models deformed at elevated confining pressure. (a) Veneer of lead and biotite exhibits folds oriented at 45 to the underlying strike slip fault (fault marked by arrows). (b) Opposite side of model in (a) shows wrench-fault system developed in limestone veneer despite isolation from forcing block by 1 mm lead layer. (c) Deformational features are displayed in a veneer of mica and lead develop over strike-slip fault (fault marked by arrows); note rotation of unconstrained mica at right side and non-rotational fault-fold system at left. (d) Thin section photo-micrograph of kink-fold in model shown in (c) displays note lead thickness change in core of fold, scale divisions are in mm. (e) thin section photo-micrograph of "normal" fault feature in model shown in (c) shows thickness change associated with lead in this feature; scale divisions are in mm. (f) Oblique view shows features produced by oblique slip on forcing-block assembly overlain by a lead-mica veneer.
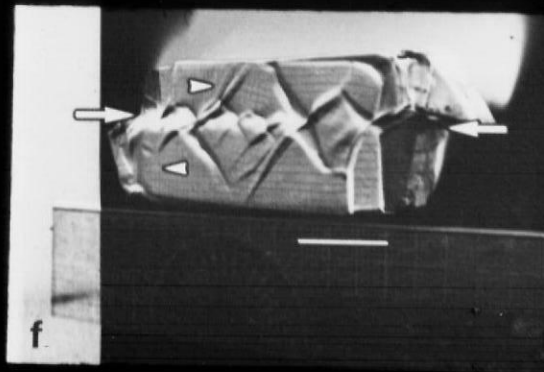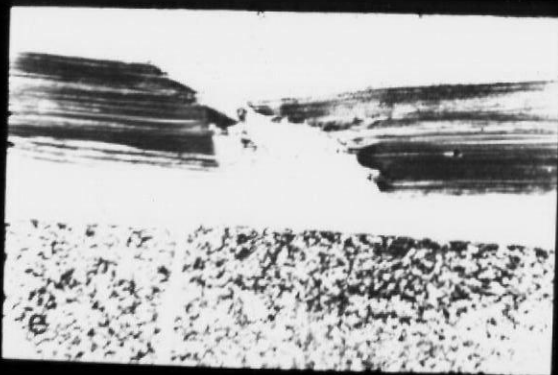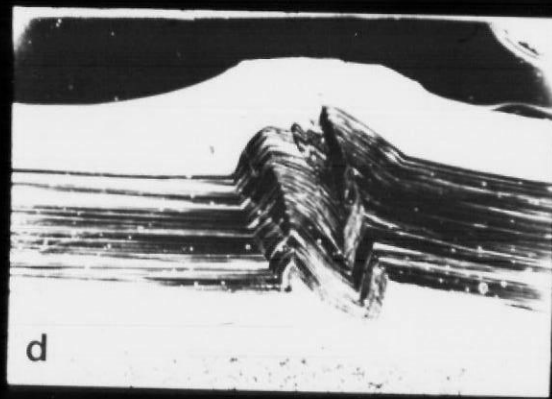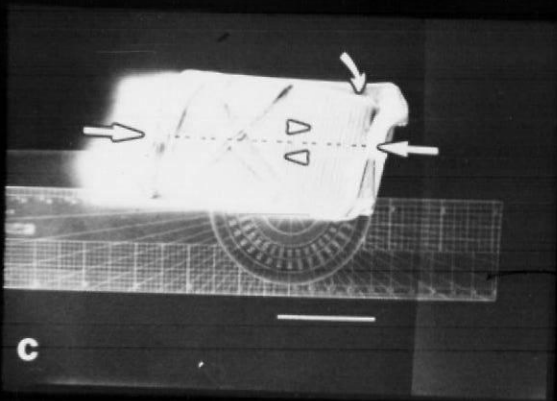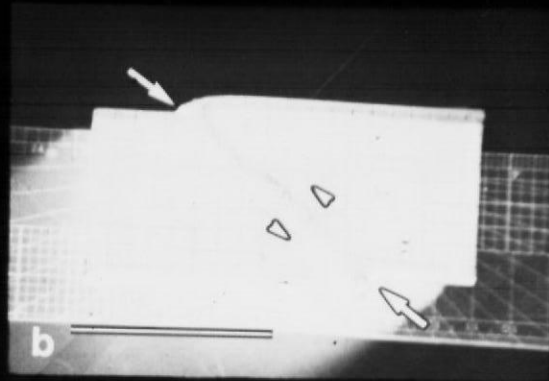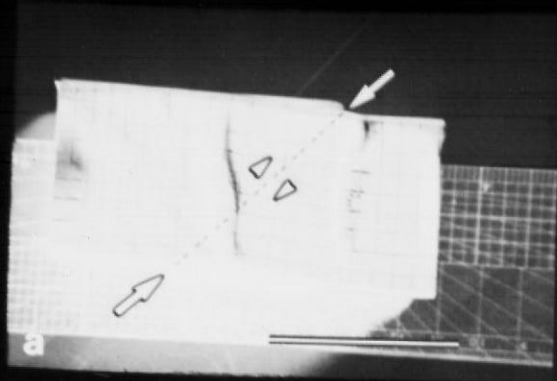
constraint (Figure 28c, p. 128). (2) In addition to the fold at approximately 45° to the fault zone (also found in model I), there are extensional faults formed. These faults are oriented normal to the fold axes. Both extension and shortening features are expected in order to maintain a non-rotational volume-consistent system. It is important to note, however, that the mica veneer in the model I did not show any extension features even though it too is non-rotational. Perhaps this is due to the additional end-load in the first model.

Thin sections made from this model exhibit thickness changes and translations on the base of the mica accommodating both extensional and shortening features (Figure 28d, e p. 127). This evidence indicates that the lead acted as an important detachment horizon for formation of those features.

A third model (model III) was designed so as to produce oblique-slip on the forcing block without end-loading the mica veneers (Appendix A). Displacement of this model results in the production of both kink folds and extensional faults similar to those described above. The difference between them is that the features are more evenly distributed along the trace of the precut than in model II, and no apparent rotations of the veneer occur. Although, there is a variation of the magnitude of vertical displacement along the precut, the average ratio of strike-slip to vertical throw is 10:1.

Comparision to Field.

The purpose behind the above series of models is to evaluate the qualitative effect of the loading conditions and the material parameters on the final geometry of the deformed layered veneer. The ultimate goal is to constrain the possible loading condition that could have produced the structures of the East Defiance Monocline.

The monocline has a sinuous strike and a northerly trend north of the point where it joins with a NE trending fault (Southwest of Window Rock, Figure 29). If the direction of hanging-wall-block-translation south of this fault intersection is normal to the mono-cline axis (Lupton area) and is the same north of the fault inter-section (Ft. Defiance) a right-lateral oblique component of motion should exist on the monocline near Ft. Definance. It is this kinematic interpretation which led to the design of the models described above. The lead and mica used for the veneer in the model represent the weak, ductile Chinle as a detachment horizon and the layered "blanket" siltstones and sandstones which overly the Chinle respectively.

The folds in the models mimic the natural folds striking about 45° to the N-S axis of the monocline in the Ft. Defiance area (Figure 29). However, there is no field indication of any NE oriented extension features on this portion of the moncline as would be predicted by models II and III. If the loading conditions for those models are valid representations of the loading conditions for

Figure 29. Map of large-scale structural features along the
East Defiance Monocline. Mapped area presented in Figures 15, p. 63
and 12, (pocket) are marked.
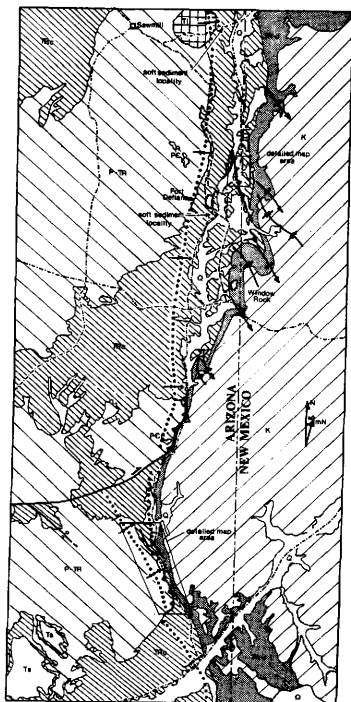
Q - Quaternary alluvial and eolean deposits

K - Cretaceous rocks: undifferentiated

TR-J - Triassic and Jurassic rocks: Wingate, Entrada, Summerville, and Morrison Fms.

TRc - Triassic Chinle Fm.

P-TR - Permian and Triassic rocks: Supai, De Chelley, and Moenkopi Fms.

PC - Precambrian crystalline rocks: granite, schist, greenstone, and phyllite in the central map area, quartzite in the northern area.

Major fault features

— sawteeth indicate hanging wall of reverse fault

— arrows indicate strike-slip movement

— U and D denote up and down sides of high angle faults

Upper monoclinal hinge

Anticlinal axis

Synclinal axis

Major roads, paved and unpaved

0   15Km

the East Defiance Monocline, then one or both of the following must explain this discrepency between model and natural features.

(1) These wrench-induced folds are in their incipient phase of development such that extensional compensating features may not have developed on the East Defiance Monocline. The anticlines and synclines which plunge obliquely off of the monocline are very low amplitude folds (averaging only about 30° difference between adjacent-limb dips).

(2) The model demonstrates that end-loading (in addition to constraint of rotation) of the mica veneer over the wrench-fault may inhibit the formation of extensional features without inhibiting formation of folds. It is possible that the natural layered section also was end-loaded during development of the observed wrench features. Perhaps this was due to hanging-wall block translation that produced a east-west horizontal end-load.

Both explanations are reasonable. Substantiation of (2) is provided by both macrofracture patterns discussed in Chapter II and dynamic microfabric data discussed in Chapter III, which point toward regional east-west oriented compression.

Regardless of the interpretation for the lack of natural extensional features, the models demonstrate adequately that large lateral translations can occur on the incompetant detachment horizon to allow subsidiary features to form adjacent to the major oblique-slip monoclinal feature. The detachment, lateral-transport, and

thickness changes that accompany ductile-detachment of the lead in the models suggests a similiar kinematic situation in the field. The effects of this kinematic development would be to produce the tectonically-induced, complex, folds and faults in the Chinle whose macroscopic character could be easily confused with that of soft-sediment structures, in the same stratigraphic position.

CHAPTER V

SUMMARY AND DISCUSSION

Summary.

Development of Structures.

The claystones and sandstones of the Chinle Formation were deposited in late Triassic time as the result of flood-plain, swamp and lake deposition. Decollement surfaces and folds 1 to over 300 m in wavelength were developed in the Chinle during deposition. These folds and faults are primarily developed in the Monitor Butte (lower) member of the Chinle. There is evidence that they were: (1) truncated by erosion and reburied by deposition of similar claystones and sandstones; then (2) in most cases subjected to shearing by movement on these shallowly buried upper and lower planer surfaces. In both cases the driving mechanism is considered to be gravity-slumping on gentle slopes. Subsequent deposition left an incomplete network of these soft-sediment structures over a large region.

The Chinle Formation then was folded and faulted during the Late Cretaceous, Laramide orogeny. The style of this deformation was controlled by its contrastingly low strength and high ductility, relative to the other formations in the section. This contrast in properties made it an ideal unit for the concentration of detachment and continuous or discontinuous (faulting) thickness changes associated with the development of monoclines. The Laramide structure

within the Chinle differs depending on whether the upthrown and downthrown displacements of the monocline are dip-slip (near Lupton) or oblique-slip (near Ft. Defiance). The latter apparently requires much more detachment and produced folds, faults and truncations in the Chinle while en echelon folds formed higher in the section. Structures from this Laramide deformation occur on the same scale and at the same location as structures of soft-sediment genesis.

An inherent characteristic of the Laramide deformation is that it occurred at a large depth of burial (2000 m) i.e., at an elevated effective confining pressure (22 MPa). Under confining pressure cataclastic and crystal-plastic deformation mechanisms operated and testify to the hard-rock nature of the deformation. Past field, laboratory and model studies covering kinematic and dynamic aspects of tectonically deformed rocks provide the background and tools used to separate hard-rock and soft-sediment features.

Criteria for distinguishing hard-rock from soft-sediment deformation.

Differentiation of soft-sediment and hard-rock deformation is accomplished by macro- and microscopic evaluation. The contrasts between the two styles of deformation are the result of differences in cementation and confining pressure at the time of deformation.

Abundant open fractures are used in the field to identify areas of probable hard-rock deformation. This is confirmed microscopically from study of thin sections cut adjacent to macrofractures. Moreover, the orientation of these fractures is consistent with the east-west maximum compression direction determined microscopically.

Soft-sediment small faults and hard-rock small-faults were observed in soft-sediment and hard-rock deformation localities, respectively. Both of these features are displacement-discontinuities of similar magni- tudes but show distinctly different characteristics. The hard-rock small-faults show reverse weathering. In thin section, there is clear evidence of grain cracking, comminution, rotation, crystal-plastic deformation, and recementation. In contrast, the soft-sediment small-faults show enhanced weathering of the fault zone due to greater clay and calcite content, and no evidence for grain cracking or crystal plastic deformation within the zone. The difference between soft-sediment small faults and hard-rock small-faults is undoubtedly due to a combination of cementation and pressure conditions during deformation.

By using (a) calcite twin lamellae, quartz deformation lamellae, microfractures and sharp extinction boundaries in quartz grains as indicators of hard-rock deformation, and (b) undeformed grains as indicators of soft-sediment deformation (or no deforma- tion), it is possible to make a relative assessment of the magnitude of gross strain responsible for the observed macroscopic deformation at any given locality. By identifying macroscopically deformed localities and analyzing populations of grains in samples from those areas, one can delineate the extent of hard-rock overprinting. In cases where both styles may be equally intense, the abundance of soft-sediment small-faults is found to be a good permanent marker of the soft-sediment deformational component.

Calcite twin lamellae, sharp extinction boundaries, deformation lamellae, microfractures, and undulatory extinctions are demonstrably Laramide features and useful to characterize the dynamics of hard-rock deformation. Dynamic interpretations of these features yield stress and strain orientations at the time of deformation which aid in interpretation of the loading conditions responsible for the deformation of each locality.

Application of Models.

Physical models are used to help clarify loading conditions and relative material responses of mechanical units which are analogs to those in the field. The physical models are useful in that they point out strengths and weaknesses of conceptual models developed from field observation.

The clay plate-bending models provide geometrical justification for the interpretation of the natural soft-sediment small-faults as a result of bending-induced stresses and strains. In addition, the two-layered model provides insight as to possible causes of alternative geometry of small faults in the tandem-layered sand units in soft-sediment localities. The clay plate-bending models fail to provide insight as to the genesis of the orthorhombic fault-array geometry observed in the field, possibly because the model is deformed only in plane-strain.

The clay-sand shear-zone model emphasizes the fallacy of assuming that the soft-sediment fold and decollement features were produced solely by simple-shear. This model helped to modify

conceptions of loading and pre-shear bed-configuration in natural shear-zones at some soft-sediment deformation localities. The important idea here is that neither the information gained from the field nor that gained from the physical models are discarded simply because of apparent contradiction. Both sets of observations are used to constrain the conceptual model of natural deformation.

The series of rock models, deformed at elevated confining pressure yield insight into the development of larger-primary and smaller-subsidiary hard-rock structures of the East Defiance Monocline. The weak, ductile layer (lead) immediately above the forcing blocks accomodates detachment and permits thickness changes, accompanying folding of the overlying units. This response is analagous to that of the Chinle in the natural deformation. Equally important is the fact that slip on layering (micas) is requisite for production of the subsidiary folds above and along the strike-slip or oblique fault. This fact is illustrated by comparison of the response of the biotite and limestone veneers on the same model assembly (Figure 28a, b, p. 127).

The features produced in non-end-loaded veneers demonstrate that extensional and compressional features are a necessary response to strike-slip faulting of underlying forcing blocks. However, the lack of extension in the end-loaded veneer provides one possible explanation for the absence of extensional features found along the East Defiance Monocline Once again field and model observations are used in a complimentary fashion to build a more accurate conceptual

model. Physical models here are not meant to bear identical corres-

pondences to the natural conterparts, simply to test certain con-

ceptions of kinematics or relative mechanical responses.

CHAPTER VI

CONCLUSIONS

Observations and analyses in this study warrant the following conclusions:

1. Deformational features of similar macroscopic style and size (chevron-folds, thrust-faults and decollements) are present in the Chinle Formation as a result of both soft-sediment and hard-rock processes and are not by themselves useful criteria for distinguishing between the two deformational-styles.

2. The two styles can be differentiated by (a) the use of both macro- and microscopic observation, of soft-sediment small-faults, hard-rock small-faults and fractures, and by (b) microscopic observation of calcite twin lamellae, sharp extinction boundaries, microfractures and quartz deformation-lamellae.

3. The intensity of soft-sediment deformation can be estimated macroscopically by the abundance of soft-sediment small-faults, which microscopically, show no grain fracturing indicating formation at low-confining pressure.

4. The intensity of hard-rock deformation can be estimated macroscopically by the abundance and orientations of

hard-rock (open) fractures and deformation bands, which microscopically, show both grain fracturing and crystal-plastic deformation indicating elevated confining pressure.

5. The intensity of hard-rock deformation can be micro-scopically estimated by the abundance of intragranular deformation features counted randomly in detrital grain populations. The microstructures are:

     i) calcite twin lamellae;

    ii) quartz deformation lamellae;

   iii) microfractures;

   iv) sharp or mosaic extinction in quartz;

    v) undulatory extinction in quartz.

6. The ordered fabric of the intragranular features listed in (5) demonstrates that they probably formed in the Chinle along the East Defiance Monocline in response to a bedding-parallel maximum principal compressive stress bearing east-west, and a minimum stress usually oriented normal to bedding,

7. Crystal-plastic features in the quartz grains produced during hard-rock deformation are more abundant than expected for the shallow depth of burial of the Chinle during deformation (Laramide).

8. Hard-rock fracture geometries are generally consistent with the microscopically determined principal stress directions.

9. The geometry of the soft-sediment soft-sediment small-faults in the Chinle may be supportive of the theory of faulting in response to a three dimensional strain boundary-condition (Oertel, 1965, and Reches, 1978).

10. Clay plate-bending models suggest that soft sediment small faults can be the direct result of bending-induced stresses and strains.

11. Rock models I, II and III, suggest that the Chinle could have acted as an important, mechanically distinctive detachment horizon during Laramide deformation. It probably was a key element in the development of thickness changes, detachment, faulting, folding and truncations observed macroscopically at the hardrock deformation locality near Ft. Defiance.

12. Rock models I, II and III also indicate that a component of right-lateral movement on the East Defiance Monocline could produce the oblique fold trends which plunge to the southeast in the Ft. Defiance vicinity, provided that slip on layering in the formations above the Chinle was sig-nificant during deformation, and that the Chinle indeed acted as a detachment horizon.

13. Applications of these criteria for differentating between soft-sediment and hard-rock deformation to other areas requires due consideration of the following:

(i)   structural stratigraphy (mechanically unique stratigraphy);

(ii) lithology used for analysis (sandstones);

(iii) scale of observation (must be both macro- and microscopic).

REFERENCES CITED

Aydin, A., 1978, Small faults as deformation bands in sandstone:
    Pageoph, v. 116, p. 913-930.

Bartlett W.L., Friedman M., and Logan, J.M., 1981, Experimental
    folding and faulting of rocks under confining pressure - Part
    IX.   Wrench faults in limestone layers: Tectonophysics,
    v. 79, p. 255-277.

Berg, R. R., 1979, Characteristics of Lower Wilcox reservoirs,
    Valentine and South Hallettsville Fields, Lavaca County,
    Texas: Gulf Coast Geological Society Transactions, v. 29, p.
    11-23.

Bishop, J. F. W., 1953, A theoretical examination of the plastic
    deformation of crystals by glide: Philosophical Magazine, v.
    44, p. 51-64.

Borg, I. and Handin J., 1966, Experimental deformation of
    crystalline rocks: Tectonophysics, v. 3, p. 249-368

Carter, N. L. and Friedman, M., 1965, Dynamic analysis of deformed
    quartz and calcite from the Dry Creek Ridge anticline,
    Montana: American Journal of Science, v. 263, p. 747-785.

Christie, J. M., Griggs, D. T., and Carter, N. L., 1964,
    Experimental evidence of basal slip in quartz: Journal of
    Geology, v. 72, p. 734-756.

Coleman, J. M., Suhayda, J. N., Whelan T., and Wright, L. D., 1974,
    Mass movements of Mississippi River deltas in Proceedings 24th
    Conference of Gulf Coast Association of Geological Societies,
    October 1974, Lafayette, Louisiana, p. 49-68.

Cook, R., 1975, Mechanisms of sandstone deformation: a study of
    the drape folded Weber Sandstone in Dinosaur National
    Monument, Colorado and Utah: Ph.D. dissertation, Texas A&M
    University.

Cooley, M. E., 1957, Geology of the Chinle Formation in the upper
    Little Colorado drainage area, Arizona and New Mexico:
    Unpublished Masters thesis, University of Arizona, 317 p.

Dunn, D. E., LaFountain, L.T., Jackson, R. E., 1973, Porosity
    dependence and mechanism of brittle franture in sandstones:
    Journal of Geophysical Research., v. 78, p. 2403-2417.

Friedman, M. 1963, Petrofabric analysis of experimentally deformed calcite-cemented sandstones: Journal of Geology, v. 71, p. 12-37.

Friedman, M., Stearns, D. W., 1971, Relations between stresses inferred from calcite twin lamellae and macrofractures, Teton anticline, Montana: Geological Society of American Bulletin, v. 82, p. 3151-3162.

Friedman, M., Hugman, R. H. H., Handin, J., 1980, Experimental folding of rocks under confining pressure, Part VIII - Forced folding of unconsolidated sand and of lubricated layers of limestone and sandstone: Geological Society of America Bulletin, v. 91, p. 307-312.

Friedman, M., White, M.A. 1980, Structural analysis of selected leg 59 cores, Deep Sea Drilling Project, in Kroenke, L., Scott, R., and others, Initial Reports of the Deep Sea Drilling Project, Volume 59: Washington, D.C., U.S. Government Printing Office, p. 503-508.

Green, T. E., 1956, Disturbed Chinle beds near St. Johns, Apache County, Arizona: Unpublished Masters thesis, University Texas, Austin, p. 71.

Groshong, R. H., Jr., 1972, Strain calculated from twinning in calcite: Geological Society of American Bulletin, v. 33, p. 2025-2038.

Handin, J. W., Hager, R. V., Friedman, M., and Feather, J. N., 1963, Experimental deformation of sedimentary rocks under confining pressure: pore pressure tests: American Association of Petroleum Geologists Bulletin, v. 47, p. 717-755.

Handin, J., Friedman, M., Logan, J. M., Pattison, L. J., and Swolfs, H. S., 1972, Experimental folding of rocks under confining pressure: Buckling of single-layer rock beams, in American Geophysical Union Monograph 16, p. 1-28.

Heard, H. C., 1963, Effect of large changes in strain rate in experimental deformation of Yule Marble, Journal of Geology, v. 71, p. 162-195.

Jamison, W. R., 1979, Laramide deformation of the Wingate Sandstone, Colorado National Monument: a study of cataclastic flow: Ph.D. dissertation, Texas A&M University, 170 p.

Kelley, V. C., 1967, Tectonics of the Zuni-Defiance Region, New
    Mexico and Arizona, in New Mexico Geological Society 18th
    Field Conference Guidebook, p. 28-31.

Kleist, J. R., 1974, Deformation by soft-sediment extension in the
    Coastal Belt, Franciscan Complex: Geology, v. 2, 501-504.

Norris, D. K., 1966, Structural analysis of the Queensway folds
    Ottawa, Canada: Canadian Journal of Earth Sciences, v. 4, p.
    299-321.

Oertel, G., 1965, The mechanism of faulting in clay experiments:
    Tectonophysics, v. 2, p. 343-393.

Prucha, J. J., Graham, J. A., Nickelsen, R. P., 1965, Basement
    controlled deformation in Wyoming Province of the Rocky
    Mountains Foreland: American Association of Petroleum
    Geologists, v. 49, p. 966-992.

Reches, Z., 1977., Analysis of joints in two monoclines in Israel:
    Geological Society of America Bulletin, v. 87, p. 1654-1662.

Reches, Z., 1978, Analysis of faulting in three dimensional strain
    field: Tectonophysics, v. 47, p. 109-129.

Reppening, C. A., Cooley, M. E. and Akers, J. P., 1969, Strati-
    graphy of the Chinle and Moenkopi Formations, Navajo and Hopi
    Indian Reservations, Arizona, New Mexico and Utah: U.S.
    Geological Survey Professional Paper, no. 521-B, 34p.

Sonstegaard, E., 1979, Glaciotectonic deformation structures in
    unconsolidated sediments at Os, south of Bergen: Norsk
    Geologisk Tidsskrift, v. 59, p. 223-228.

Stearns, D. W., 1968, Certain aspects of fracture in naturally
    deformed rocks, in Riecker, R.E., ed., Rock mechanics
    seminar: Bedford, Mass., Terrestrial Science Laboratories,
    Air Force Cambridge Research Labs., Contract AD 669375, v. I,
    p. 97-118.

Stewart, J. H., Poole, F. G., Wilson, R. F., Cadigan, R. A.,
    Thordarson, W., Albee, H. F., 1972, Stratigraphy and origin of
    the Chinle Formation and related Upper Triassic strata in the
    Colorado Plateau Region: U.S. Geological Survey Professional
    Paper, no. 690, 336 p.

Straccia, J. R., The stratigraphy and structure of the Rosita Gas
    Fields, Duval County, Texas: Unpublished Masters Thesis,
    Texas A&M University, 74 p.

Swolfs, H. S., 1971, Influence of pore fluid chemistry and
    temperature on fracturing of sandstone under confining
    pressure: Ph.D. dissertation, Texas A&M University, 160p.

Thomsen, A., 1969, Soft-sediment fault in the Tesnus Formation and
    their relationship to paleoslope, in McBride, E.F., ed.
    Dallas Geological Society Guidebook to the Stratigraphy,
    sedimentary structures and origin of flysch and preflysch
    rocks of the Marathon Basin, Texas, p. 72-77.

Turner, F. J., 1953, Nature and dynamic interpretation of
    deformation lamellae in calcite of three marbles: American
    Journal of Science, v. 251, p. 276-298.

Vaughn, P. H., 1976, Mesozoic sedimentary rock features resulting
    from volume movements required in drape folds at corners of
    basement blocks - Casper Mountain area, Wyoming: Unpublished
    Masters Thesis, Texas A&M University, 93 p.

Wienberg, D. M., 1977, Two-dimensional kinematic analyses of
    selected aspects of folding in the Rocky Mountain foreland,
    and their geologic implications: Ph.D. dissertation, Texas
    A&M University, 111 p.

Wilcox, R. E., Harding, T.P., Seely, D.R., 1973, Basic wrench
    tectonics: American Association Petroleum Geologists
    Bulletin, v. 57, p. 74-96.

Wilson, R. C., Jr., 1970, The mechanical properties of the shear
    zone of the Lewis Overthrust, Glacier National Park, Montana:
    Ph.D. Dissertation, Texas A&M University, 88 p.

APPENDIX

HIGH-PRESSURE MODEL EXPERIMENTAL CONFIGURATIONS

Three different models were used to test the effect of wrench
and oblique forcing-block motions on overlying veneers (Figure
30). The veneers are isolated mechanically from the forcing-blocks
by a veneer of low-strength lead. Note that model I is the only
model that allows end loading of the veneers and that model III is
the only one that produces oblique-slip. (Figure 30). In Figure
30 piston motions are indicated by arrows.

Figure 30. High-pressure model experimental configurations.

STRIKE-SLIP
ALL VENEERS END-LOADED

MODEL I

3MM THICK BIOTITE
2MM THICK LEAD
1.5CM THICK SANDSTONE
    FORCING-BLOCK
2MM THICK LEAD
3MM THICK LIMESTONE

[2CM

STRIKE-SLIP
VENEERS NOT END-LOADED

MODEL II

2.5MM THICK MUSCOVITE
1MM THICK LEAD
1CM THICK SANDSTONE
    FORCING-BLOCK
1MM THICK LEAD
10-.1MM MUSC. SHEETS

[2CM
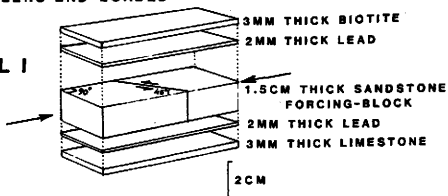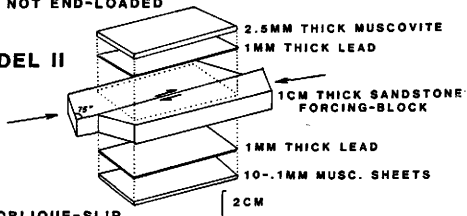
OBLIQUE-SLIP
VENEERS NOT END-LOADED

MODEL III

10-.1MM MUSC. SHEETS
1MM THICK LEAD
1CM THICK SANDSTONE
    FORCING-BLOCK
1MM THICK LEAD
7-.1MM MUSC. SHEETS

[2CM
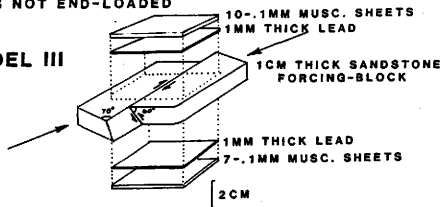
VITA

NAME: Jay Roger Scheevel

BORN: September 6, 1957, in Grand Junction, Colorado

PARENTS: Robert Warren and Janet Spurgeon Scheevel

EDUCATION: University of Illinois, Champaign/Urbana
                 B.S. Geology, 1979

PROFESSIONAL EXPERIENCE:

        Summer, 1979:   Uranium Geologist
                         USGS Uranium and Thorium Branch
                         Golden, Colorado

        1979-1980:   Graduate Teaching Assistant
                         Texas A&M University
                         College Station, Texas

        Summer, 1980:   Uranium Geologist
                         Exxon Minerals, Exxon U.S.A.
                         Casper, Wyoming

        1981-Present: Exploration Geologist
                         Chevron USA, Central Region
                         Denver, Colorado

ADDRESS: c/o Chevron USA
                 P.O. Box 599
                 Denver, Colorado 80207

KEY

Q Quaternary deposits
Qls mass landslide deposits

K Cretaceous rocks undifferentiated

R-J Jurassic-Triassic rocks undiferentiated

Chinle Fm.

Ɍco Owl Rock Mbr.
Ɍcpu Upper Petrified Forest Mbr.
Ɍcps Sonsella Sandstone
Ɍcpl Lower Petrified Forest Mbr.
Ɍcm Monitor Butte Mbr.
Ɍcs Shinarump Mbr.

Ɍm Moenkopi Fm.

Pdc De Chelley Fm.

upper monoclinal hinge

major roads   drainage

FRACTURE STRIKES

n=28

n=18

n=36

MEASURED SECT. 3

MEASURED SECT. 2

MEASURED SECT. 1

LINE OF SECTION

N

scale

0   1 km   2   3   4

FIGURE 15, JAY ROGER SCHEEVEL, 1983

Map of structural features in the Lupton area, Arizona

FRACTURE STRIKES

INDEX LETTER IDENTIFIES
STATION LOCATION
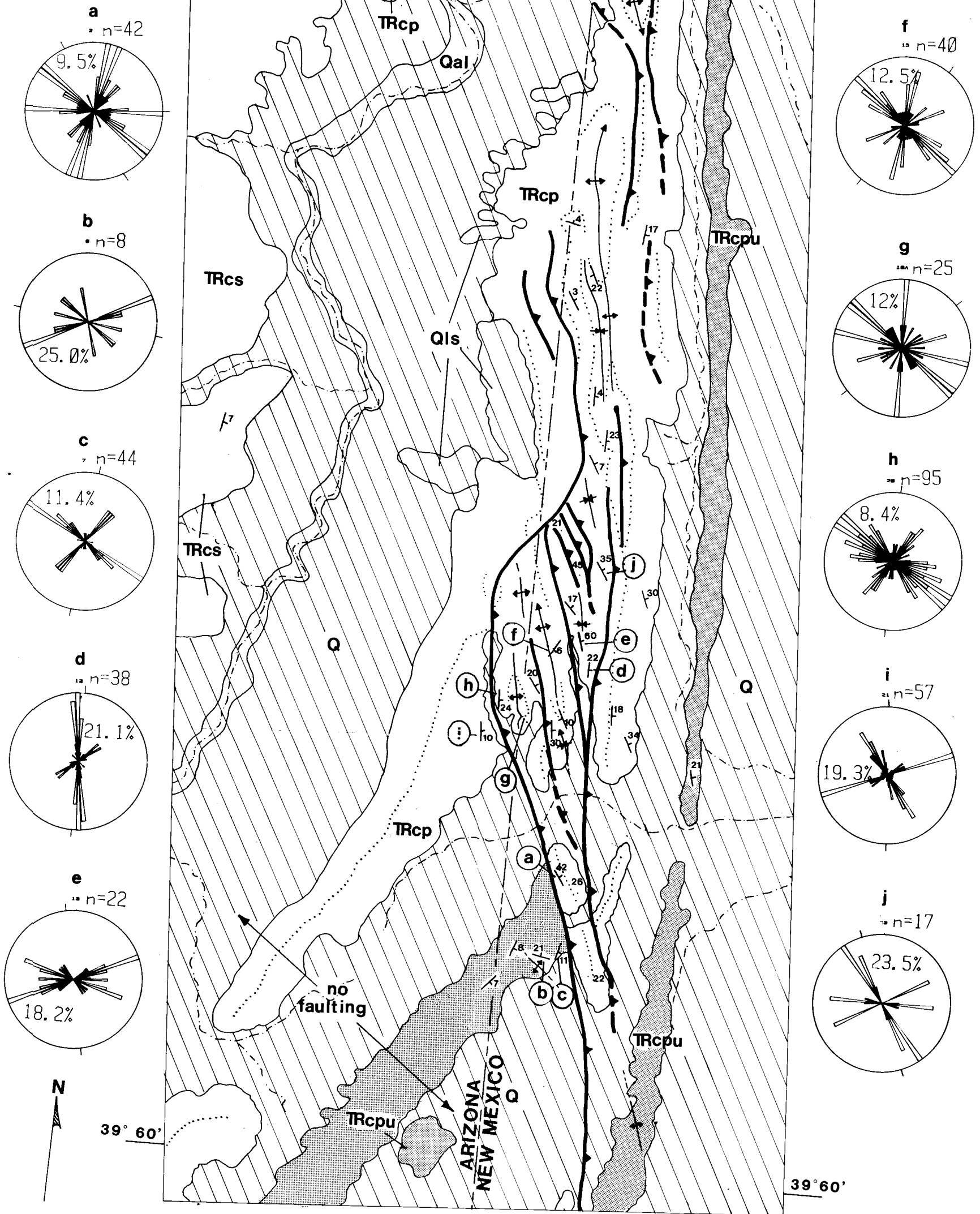
a n=42
9.5%

b n=8
25.0%

c n=44
11.4%

d n=38
21.1%

e n=22
18.2%

f n=40
12.5%

g n=25
12%

h n=95
8.4%

i n=57
19.3%

j n=17
23.5%

N

TRcp
Qal
TRcp
TRcs
Qls
TRcs
Q
TRcpu
Q
TRcp

no
faulting

TRcpu

ARIZONA
NEW MEXICO
Q

39° 60'

39°60'

KEY

Q	Quaternary deposits
Qal	alluvial deposits
	landslide deposits

Chinle Fm.

TRcpu Upper Petrified Forest Mbr.

TRcp Petrified Forest Mbr. undif.
(primarilly Sonsella Sandstone)

TRcs Shinarump Mbr.

resistant weathering strata

thrust faults (dashed where inferred)

anticlinal axes

synclinal axes

SCALE

0   0.5   1.0Km

FIGURE 12, JAY ROGER SCHEEVEL, 1983

Map of hard-rock structural features
3 km northeast of Ft. Defiance , Arizona